2015

Smoke Characterization and Feasibility of the Moment Method for Spacecraft Fire Detection

Marit E. Meyer
NASA Glenn Research Center, Cleveland, Ohio, USA, marit.meyer@gmail.com

George W. Mulholland
University of Maryland, College Park, Maryland, USA

Victoria Bryg
National Center for Space Exploration Research, Cleveland, Ohio, USA

David L. Urban
NASA Glenn Research Center, Cleveland, Ohio, USA

Zeng-guang Yuan
National Center for Space Exploration Research, Cleveland, Ohio, USA

See next page for additional authors

Aerosol Science and Technology, 49:299–309, 2015
ISSN: 0278-6826 print / 1521-7388 online
DOI: 10.1080/02786826.2015.1025124

Smoke Characterization and Feasibility of the Moment Method for Spacecraft Fire Detection

Marit E. Meyer,[1] George W. Mulholland,[2,3] Victoria Bryg,[4] David L. Urban,[1] Zeng-guang Yuan,[4] Gary A. Ruff,[1] Thomas Cleary,[3] and Jiann Yang[3]

[1]*NASA Glenn Research Center, Cleveland, Ohio, USA*
[2]*University of Maryland, College Park, Maryland, USA*
[3]*National Institute of Standards and Technology, Gaithersburg, Maryland, USA*
[4]*National Center for Space Exploration Research, Cleveland, Ohio, USA*

The Smoke Aerosol Measurement Experiment (SAME) has been conducted twice by the National Aeronautics and Space Administration and provided real-time aerosol data in a spacecraft micro-gravity environment. Flight experiment results have been recently analyzed with respect to comparable ground-based experiments. The ground tests included an electrical mobility analyzer as a reference instrument for measuring particle size distributions of the smoke produced from overheating five common spacecraft materials. Repeatable sample surface temperatures were obtained with the SAME ground-based hardware, and measurements were taken with the aerosol instruments returned from the International Space Station comprising two commercial smoke detectors, three aerosol instruments, which measure moments of the particle size distribution, and a thermal precipitator for collecting smoke particles for transmission electron microscopy (TEM). Moment averages from the particle number concentration (zeroth moment), the diameter concentration (first moment), and the mass concentration (third moment) allowed calculation of the count mean diameter and the diameter of average mass of smoke particles. Additional size distribution information, including geometric mean diameter and geometric standard deviations, can be calculated if the particle size distribution is assumed to be lognormal. Both unaged and aged smoke particle size distributions from ground experiments were analyzed to determine the validity of the lognormal assumption. Comparisons are made between flight experiment particle size distribution statistics generated by moment calculations and microscopy particle size distributions (using projected area equivalent diameter) from TEM grids, which have been returned to the Earth.

Received 11 September 2014; accepted 17 February 2015.
Address correspondence to Marit Meyer, Combustion Physics and Reacting Processes Branch, NASA Glenn Research Center, 21000 Brookpark Road, Cleveland, OH 44135, USA. E-mail: marit.meyer@nasa.gov

INTRODUCTION

SAME Experiment

Appropriate design of fire detection systems requires knowledge of both the expected signature of the events to be detected and the background levels. Ambient aerosols in spacecraft include significantly larger particles than on the Earth, as gravitational settling is absent; consequently, smoke detectors must optimally distinguish between background aerosols and smoke in order to prevent false alarms. Terrestrial fire detection systems have been developed based on extensive study of terrestrial fires (Bukowski and Mulholland 1978; Bukowski et al. 2003). Unfortunately, there is no corresponding dataset for spacecraft fires, and consequently the fire detectors in current spacecraft were developed based upon terrestrial designs. There are a number of factors that could be expected to affect the particle size distribution of the smoke from spacecraft fires. In low gravity, buoyant flow is negligible, which increases particle residence time in microgravity fires and increases the transport time from the reaction zone to detectors (Brooker et al. 2007). Microgravity fires can have significantly different structure from their 1-g counterparts, which can change the formation history of smoke particles. Finally, the materials used in spacecraft are different from typical terrestrial environments where smoke properties were previously evaluated. All of these effects can influence the smoke particle size distribution. The objective of Smoke Aerosol Measurement Experiment (SAME) was to make sufficient measurements of smoke in space to enable improved design of future fire detectors.

It is critically important to detect a fire in its early phase before a flame is established, given the constrained volume on any spacecraft. Consequently, the primary target for spacecraft fire detection is pyrolysis products rather than soot. Therefore, SAME was designed to characterize smoke from overheating

samples (oxidative pyrolysis) rather than from flaming combustion. Detectors used on the Space Shuttle were based upon ionization fire detector technology, the most advanced technology available at the time and used an inertial separator designed to eliminate particles larger than 1–2 μm. The International Space Station (ISS) smoke detectors use near-infrared (IR) forward scattering, rendering them most sensitive to particles larger than 1 μm outside the range of sensitivity of the shuttle detector.

The SAME was developed to obtain smoke particle size distribution parameters on orbit without returning samples to the Earth. This is a challenging endeavor because existing aerosol instruments are typically large and incompatible with spacecraft experiment constraints. Space experiments cannot require extensive crew training, equipment calibration, or maintenance and instruments must have low power requirements, be compact, lightweight, and easily assembled and disassembled. The approach for SAME was to use three commercial off-the-shelf instruments to measure different moments of the smoke particle size distribution. Using these moments, different moment average diameters can be calculated (some of which require assumption of a lognormal distribution) and the smoke aerosol can be characterized for the benefit of future smoke detector design. The measurements were made on smoke generated by overheating materials commonly found on spacecraft with controlled sample temperatures, flow rates, and particle aging times. Materials tested include Teflon®,[1] Kapton®, cotton lamp wick (cellulose, representative of paper, wood, and fabric), silicone rubber, and Pyrell®, a polyurethane foam. The experiment was designed to measure fresh and aged pyrolysis smoke because the likely origin of a spacecraft fire would be electronics in an avionics enclosure or other poorly ventilated region. In such a scenario, the smoke concentration would increase in the confined space before escaping into the cabin where large-scale forced turbulence would slowly dilute the smoke. Thus, the properties of early and aged smoke should be known for optimal fire detector design. The experiment was performed in space in 2007 and 2010 on the ISS. The purpose of this article is two-fold: (1) Report the pyrolysis smoke characteristics of common spacecraft materials to inform future fire detector design, and (2) evaluate the feasibility and limitations of using combined moments for measuring smoke aerosol size distribution parameters in low gravity, particularly the validity of the lognormal assumption. A companion article (Mulholland et al. 2015) discusses other aspects of the SAME smoke, such as pyrolysis rate, smoke plume structure, yield, and particle structure.

[1]Certain commercial equipment, instruments, or materials are identified in this article to foster understanding. Such identification does not imply recommendation or endorsement by the National Aeronautics and Space Administration (NASA) or the National Institute of Standards and Technology, nor does it imply that the materials or equipment identified are necessarily the best available for the purpose.

Moment Method

The approach used by the SAME experiment is termed the "moment method" for convenience (Cleary et al. 2003). Three moments of the smoke particle size distribution (zeroth, first, and third moments) were measured, and using the properties of the lognormal distribution, the geometric mean diameter and the standard deviation of the aerosol were calculated. The following two assumptions are made when using this method: The aerosol particles have a spherical (or nearly spherical) shape, and the size distribution is lognormal.

We provide a detailed overview of the moment method in the online supplemental information (SI). Relevant formulas used for data in this study are repeated here without elaboration. The zeroth moment (M_0) is equal to the total number concentration, N_{tot}. When particles can be characterized as spherical, the first moment (M_1) is equal to the total diameter length concentration, or the integrated diameter per unit volume, L_{tot}, and the third moment (M_3) is proportional to the total volume and/or mass concentration ($M_{tot} = \pi\rho M_3/6$), which includes the particle density.

Thus, one can obtain the commonly used count mean diameter (simple average), d_{av}, and the diameter of average mass, d_m:

$$d_{av} = \left(\frac{M_1}{M_0}\right) = \frac{L_{tot}}{N_{tot}}, \quad [1]$$

$$d_m = \left(\frac{M_3}{M_0}\right)^{1/3} = \left(\frac{6M_{tot}}{\pi\rho N_{tot}}\right)^{1/3}. \quad [2]$$

There is no assumption about the form of the size distribution for Equations (1) and (2). However, to determine the geometric standard deviation, σ_g, of the size distribution, or other moment diameters by the moment method, requires that the size distribution be lognormal and that the particles be spherical. The lognormal distribution is widely used for describing aerosols, including non-flaming smoke because for most smoke aerosols, the bulk of the number concentration is associated with smaller particles (Raabe 1971; Reist 1984). Many studies have assumed that pyrolysis and combustion smoke aerosols from various fuels have a lognormal size distribution (Chen et al. 1990; Li and Hopke 1993; Zai et al. 2006; Xie et al. 2007; Chakrabarty et al. 2010; Janhäll et al. 2010; Mack et al. 2010).

The general formula for the pth moment average of the qth moment distribution is

$$d_{p,q} = d_g \exp\left[\left(q + \frac{p}{2}\right)\ln^2\sigma_g\right], \quad [3]$$

where σ_g is the same for particle number and volume distributions, and d_g is equal to the count median diameter of the distribution and is the same as the geometric mean diameter if the lognormal assumption is satisfied.

If a histogram of particle sizes is available, the diameter of an average property proportional to $(d_p)^p$ can be calculated for i bins with the following formula:

$$d_p = \left(\frac{\sum n_i d_i}{N}\right)^{1/p}. \quad [4]$$

With this formula, binned data from a reference instrument can be used to verify results from moment method calculations.

Aerosol instruments are limited in their range of measurements, and the accuracy of the measurements may vary over the range as well. If the moments of the particle size distribution are determined by instruments that are not identical in their ranges of particle size measurement, we can quantify the truncated moment value normalized by the total moment value. This relative value indicates how much of an actual signal is captured in the limited detection range of an instrument. The formula for a bounded moment measurement, which assesses the uncertainty induced by an instrument omitting particles above or below a certain diameter D, is based on the pth moment cumulative function of a lognormal distribution with d_g and σ_g. If D is the particle size below which no signal can be detected, the relative cumulative pth moment is,

$$M_{p,\mathrm{rel}} = \frac{1}{2}[1 + \mathrm{erf}(\eta_D)], \text{where } \eta_D = \frac{\ln\left(\frac{D}{d_g}\right)}{\sqrt{2}\ln\sigma_g} - \frac{1}{\sqrt{2}}p\ln\sigma_g. \quad [5]$$

The derivation of this equation is given in the online Supplemental Information. Note that the limiting diameter D is normalized by d_g. This relative cumulative moment function, $M_{p,\mathrm{rel}}$ gives the percentage of the pth moment instrument signal that is captured when particles smaller than a diameter D cannot be detected, assuming a lognormal distribution with d_g and σ_g. Conversely, when $M_{p,\mathrm{rel}}$ is subtracted from 1, it gives the percentage of the instrument signal that is lost due to lack of instrument range beyond diameter D.

SAME Aerosol Instruments

The SAME flight and ground test experiment measurements were made using three commercial instruments, which had been ruggedized and re-packaged for space flight. Two are industrial hygiene instruments and one is a residential smoke detector. These instruments were chosen because of their simplicity, low power needs, and small size. Unfortunately, they all show material or size-dependent behavior. Detailed empirical calibrations were performed with these instruments, which are described in the SI along with additional information on the instruments.

The zeroth moment instrument is a P-Trak™ (TSI, Shoreview, MN, USA), which is a condensation particle counter that was modified for use in space because the isopropanol condensate does not flow downwards to the wick in low gravity (Urban et al. 2005). To mitigate this issue, very small grooves were added to the walls of the condensing section of the device to improve conductance of condensate back to the wick. The first moment instrument is the ionization chamber from a residential smoke detector. This device uses an alpha-particle emitter to generate ions in a region within a DC electric field. Drifting ions in the electric field results in a current, and the presence of aerosol particles reduces the current as a result of the attachment of ions to particles. The mobility of the charged aerosol is too small for it to be collected on the ionization chamber electrode. Required minimum particle concentrations are of the order of 10^5 particles/cm^3 and no sample dilution is required. The SAME third moment instrument is the DustTrak™ (TSI, Shoreview, MN, USA), which is a nephelometer using a 90° light scattering signal with a wide acceptance angle and output calibrated to quantify the aerosol mass concentration of Arizona Test Dust (ISO 12103-1). Material-specific calibrations and corrections were needed to account for the range of particle sizes, shapes, and refractive indices in the SAME experiment, and the particle density was required to compute M_3 from the mass concentration. While some studies have shown that the DustTrak™ response is not proportional to mass (Moosmüller et al. 2001; Maricq 2013), after applying calibration factors, the DustTrak™ was found to correlate with the mass concentration. The calibration factors with uncertainty are given in the companion article by Mulholland et al. (2015). Some smoke could be sent to an autonomously operated thermal precipitator in which smoke particles are deposited on transmission electron microscope (TEM) grids. The SAME software command caused a valve to open, diverting smoke into one of the 12 isolated ducts containing a heated Kanthal wire above the TEM grid. Additional details on the thermal precipitator design are in the online Supplemental Information. After the space flight experiments, six thermal precipitators were returned to the Earth, and the grids were examined in a TEM to observe particle morphology and to obtain particle size distributions by microscopy. Characterization of particle morphology is a key to determining whether the moment method is valid for obtaining d_g and σ_g from d_{av}, and d_m.

A schematic of the SAME hardware appears in Figure 1. Space experiments are ideally autonomous, with minimal astronaut intervention beyond initial assembly. Hardware with programmable experiment parameters decreases crew-training requirements and increases the quantity and reliability of the resulting data. Software controlled all aspects of the experiment once the crew inserted the fuel sample carousel and commenced the test sequence. For the space experiments, smoke was generated by overheating a small sample of material in the smoke generation duct for approximately 60 seconds.

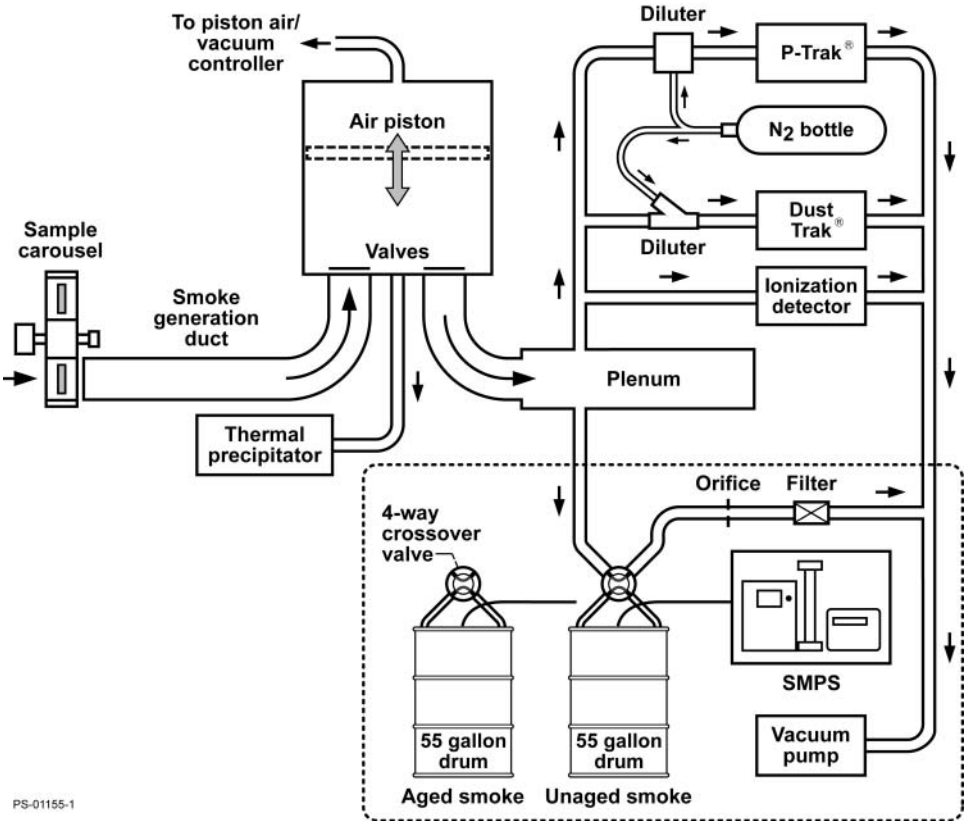

FIG. 1. SAME flight hardware schematic, shown with additional ground testing apparatus within the dotted line. During ground tests, some smoke is diverted from the SAME setup to fill one of the two drums, which hold the diluted smoke for SMPS measurements. Two drums were needed to contain and measure both unaged and aged smoke.

During this interval, a rising piston drew smoke into a 6-liter aging chamber, where it could be held for a predetermined aging duration, allowing the particles to coagulate. Half of the smoke was pushed by the piston into moment instruments almost immediately for unaged smoke measurements by moment instruments. After a period of aging, the remaining smoke was measured. Additional information on the sample heating sequence and temperatures is given in the companion article (Mulholland et al. 2015).

SAME Smoke-in-Drums Ground-Based Experiment

In order to assess whether the size distribution of a particular smoke is lognormal, detailed particle size distributions were measured with a reference instrument. This cannot be accomplished in low gravity, so this investigation was performed with the ground-based engineering SAME hardware, which is identical to the setup on the ISS, incorporating the flight aerosol instruments that had been returned to the Earth. A Scanning Mobility Particle Sizer (SMPS) Spectrometer (3936, TSI, Shoreview, MN, USA) was used as the reference instrument in the validation experiment. The SMPS requires a two-minute scan through a range of voltages to acquire a high-resolution particle size distribution; however, the duration of smoke supplied from the SAME aging chamber is at most 30 seconds. Therefore, the smoke was collected in an intermediate container, which served two purposes. The first purpose was to sufficiently dilute the smoke from the SAME chamber to effectively stop coagulation (aging) of smoke particles during the SMPS scans. The second purpose was to have a large enough quantity of diluted smoke for multiple SMPS scans. A 55-gallon drum was chosen for this purpose and the SAME smoke-in-drums setup was developed to enable SMPS measurements on a portion of smoke output from the SAME piston chamber. The configuration is shown in Figure 1, which shows the original SAME hardware outside the dashed outline. One DustTrak^{TM} was removed from the original SAME configuration and its portion of the smoke sample was diverted from the setup to one of the two drums which hold the diluted smoke during multiple two-minute SMPS measurements. One drum collected fresh smoke from the heated sample material and the other was filled after a controlled aging period in the piston chamber. Thus, both aged and unaged smoke could be measured with SMPS. Unfortunately, one or more of

the flight moment instruments was not functioning properly during these ground-based tests, so a majority of the resulting moment data were not reliable. Therefore, the analysis of the drum test data is exclusively on SMPS results, particularly to assess whether smoke from different test materials can be assumed to have a lognormal particle size distribution. While a comparison of the moment data with the SMPS reference data would have been preferable, lognormality is a fundamental assumption of that approach, and needs to be confirmed or refuted before spacecraft fire detection systems are further developed.

RESULTS

The results of the various aerosol measurements are presented in the following order: TEM images of low-gravity particle morphology which influences interpretation of the results of the moment instruments. SMPS smoke particle size distributions from ground testing provide a visual means of determining whether the smoke particle sizes are lognormally distributed, and discrete SMPS particle bin data are used to further test for lognormality. TEM particle size distributions from flight tests are given for materials with sufficient particle deposition in the thermal precipitator and provide an independent reference for moment method results.

TEM Particle Morphology Results from Flight Tests

Summaries are given on the morphology of all five materials tested, and details on the pyrolysis and formation are in the companion article (Mulholland et al. 2015). Kapton particles are the smallest of the five materials tested and are rarely agglomerated. The spherical shape and uniform density indicate growth by condensation in the saturated vapor of pyrolysis products. Figure 2 shows the effect of aging, with the unaged particles (Figure 2a) having a higher population of very small particles, and the aged ones (Figure 2b) appearing only slightly larger.

Lamp wick smoke aerosols (Figure 2c) are known to be primarily spherical droplet-type particles that grow by condensation of pyrolysis gases (Mulholland 1995). Occasional doublets are seen but most are unagglomerated. Two distinct large particle types are observed: uniformly dense or lighter in the center, which suggests that they arrive at the carbon film of the TEM grid as a liquid. Some TEM images display additional faint particles that covered only one or two pixels.

Pyrell smoke particles (Figure 2d) comprise agglomerates made up of primary particles ranging from 30 to 100 nm. Teflon primary particles are much smaller and are agglomerates with a fractal structure (Figure 2e). The darker agglomerates are more electron-dense and indicate that the fainter particles may have partially evaporated in the electron beam. In

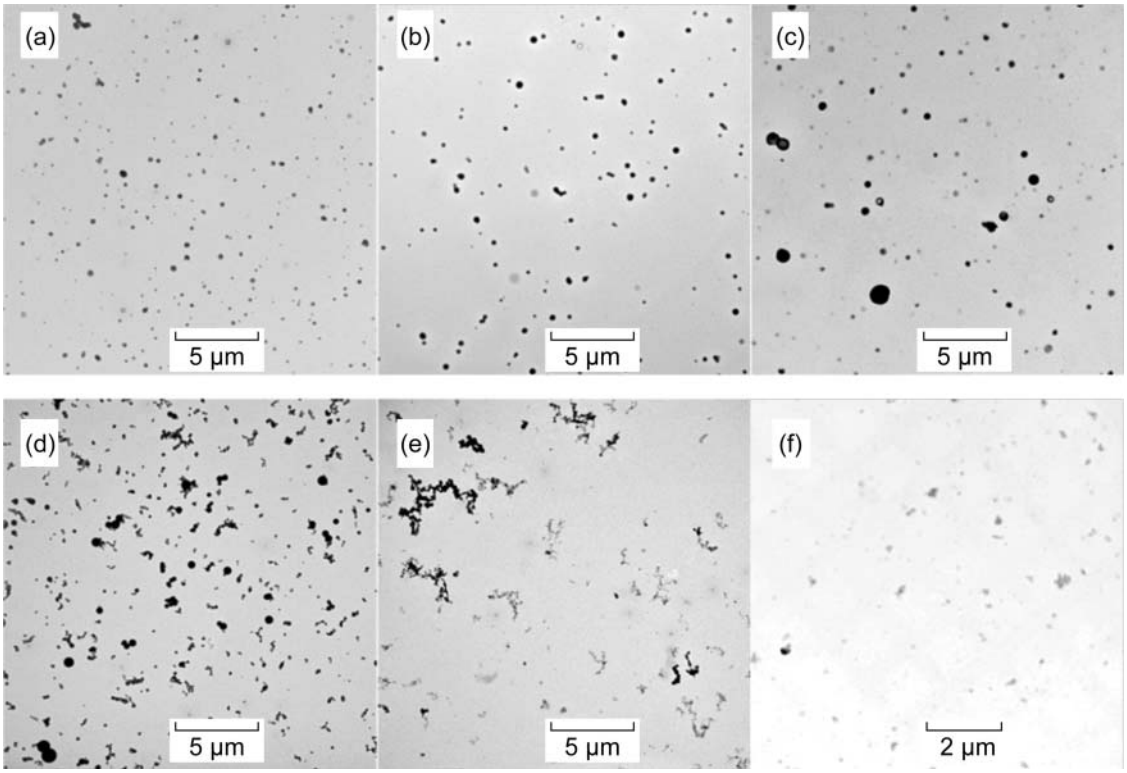

FIG. 2. TEM images showing morphology of smoke particles from ISS testing, all with a reference length scale = 5 μm, with the exception of image (f). (a) Unaged Kapton 574°C, (b) aged Kapton 574°C, (c) Unaged lamp wick, 265°C, (d) Unaged Pyrell, 242°C, (e) Unaged Teflon, 514°C, and (f) ISS residual unaged silicone smoke particles, 380°C, and reference length scale = 2 μm.

addition, some particles were not completely adhered to the TEM grid and movement could be observed as the force of the electron beam influenced the loose ends of agglomerates.

Silicone particles were not wholly preserved on the TEM grids owing to the volatile nature of pyrolysis products. Only very small and faint particles remained after the return flight to the Earth, as seen in Figure 2f. Note that the magnification in this figure is nearly double that of the other particle images shown. SMPS ground test data indicate that fresh silicone particles are much larger, as seen in Figure 3e.

Morphology results show that only Kapton and lamp wick are spherical aerosols, so they are better suited to calculating particle diameters from TEM images. Although the TEM images of silicone do not reflect spherical morphology, it is considered a spherical smoke aerosol as it consists of liquid droplets (Mulholland 1995). Regardless of shape, meaningful values of d_{av} can be calculated from moment instrument results, and the material-specific calibration of the DustTrak with fundamental aerosol mass measurements provides moment method values for d_m, which are valid for the nonspherical materials, Pyrell and Teflon (by Equations (1) and (2)). No significant discernable difference was noted between the morphology of the pyrolysis particles sampled in low gravity versus normal gravity for typical SAME flow conditions. A specific set of test points were run in low gravity with no flow through the SAME smoke generation duct, which resulted in significantly larger spherical particles. Details of these tests are outlined in the companion article (Mulholland et al. 2015).

SMPS Results for Spherical Smoke Aerosols

Five SAME materials were tested at two temperature levels: baseline and high temperature. Typical particle size distributions from the ground testing validation experiments of the unaged and aged smoke for more spherical aerosols are shown in Figure 3. Pyrell® and Teflon® are not spherical aerosols and are not analyzed here; however, their mobility diameter size distributions appear in the SI. Particle size distributions are shown in the upper plots, Kapton (Figure 3a), lamp wick (Figure 3c), and silicone (Figure 3e). The plotted lines represent a lognormal curve-fit with the MATLAB Statistics Toolbox function "nlinfit," which performs nonlinear least squares regression with the Levenberg–Marquardt algorithm (MATLAB version R2012a, The MathWorks Inc.). Residual plots are aligned directly below the size distributions showing deviations from lognormal fits. This visual test for "goodness-of-fit" would result in randomly scattered residual points, both above and below zero, for a good lognormal fit. It is common to observe a wedge-shaped spread of residuals, as in Kapton (Figure 3b), where the tails of the distribution have mostly small residual values, with a wider spread of residuals around the peak diameter. In general, the spread of the residuals is more compact for Kapton and lamp wick, indicating a better lognormal fit for these materials. Note that the unaged Kapton residuals are mostly positive up to 70 nm, which indicates that the data are less steep than the lognormal fit. The lamp wick residual plot (Figure 3d) also shows a small but systematic deviation from the lognormal fit, which is evident by the change in sign of the unaged data residuals between 500 nm

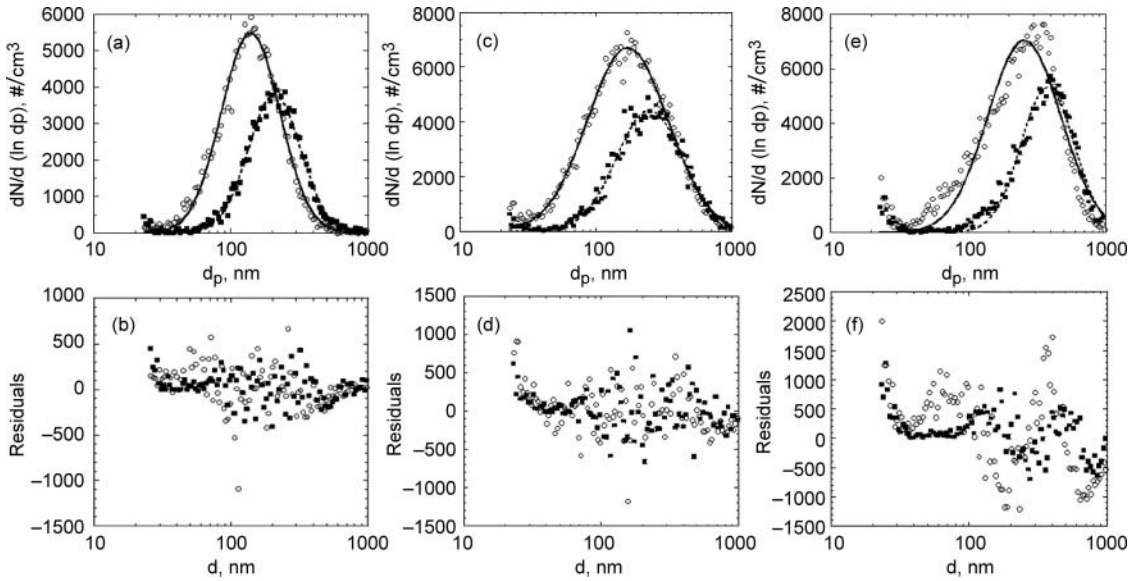

FIG. 3. Ground testing size distributions and residual plots for Kapton (a, b), lamp wick (c, d), and silicone (e, f). Upper images are SMPS measurements, open markers for unaged smoke, and solid for aged; solid curves represent the nonlinear least square fits. Size distribution parameters: (a) Kapton® baseline temperature test (510°C), unaged $dg = 139$ nm, $\sigma g = 1.78$, aged $dg = 209$ nm, $\sigma g = 1.66$. (c) Lamp wick high-temperature test (286°C), unaged $dg = 171$ nm, $\sigma g = 1.98$, aged $dg = 248$ nm, $\sigma g = 1.75$. (e) Silicone baseline temperature test (342°C), unaged $dg = 257$ nm, $\sigma g = 1.84$, aged $dg = 382$ nm, $\sigma g = 1.56$. Residual plots of deviations from lognormal fits are aligned below each size distribution.

and 600 nm. The silicone residual plot (Figure 3f) shows the least randomness, which indicates that the lognormal fit is less valid. The residuals change signs on both sides of the peak, indicating a shoulder in the small sizes (residuals go from positive to negative), the peak is offset from the fit (positive residuals around 400 nm), and the data are steeper than the lognormal fit in large sizes (negative residuals). Furthermore, the silicone residual plot has more noise and negative residuals at higher diameters, which may also be caused by losses from gravitational settling of these larger particles in the SAME aging chamber and/or the 55-gallon drum. Several systematic deviation patterns are observed, for example, where a shoulder in the distribution exists, a corresponding set of all positive residuals show a marked departure from the lognormal curve fit. This could be attributed to an improper multiple charge correction.

It is notable that most of the extreme positive and negative values of the residuals for all materials are for unaged smoke (open symbols), which suggests that as smoke ages within the timeframe of this experiment, it becomes more lognormal. As expected, the aged (black symbol) distribution moves to the right as aging increases the geometric mean diameter and σ_g decreases as the distribution narrows by coagulation. Log-probability plots were also used to assess lognormality of these aerosols in the SI.

The SMPS setting for a 10:1 sheath-to-aerosol flow rate ratio (3.0-lpm sheath, 0.3-lpm aerosol flow) captured the complete size distribution only for unaged Kapton® smoke, whereas other materials had larger size ranges, which were only completely captured by a 5:1 flow rate ratio (1.5-lpm sheath, 0.3-lpm aerosol flow) which extended the measurement range to 1000 nm. Silicone and Teflon® high temperature distributions were not completely captured by SMPS, even with a larger range of up to 1000 nm. Some SMPS distributions had an initial uptick in the small diameter tail, which is believed to be a sampling anomaly in the SMPS, possibly an artifact from the previous sample, as the scans were performed in rapid succession. This anomaly did not have a significant effect on the parameters obtained in the fitting of SMPS data.

TEM Particle Size Distribution Results

Particle size distributions were created by image analysis of the particles captured on TEM grids as an independent verification of particle measurements and moment diameter calculations. The particle-projected area-equivalent diameter was computed, which is considered to be equivalent to mobility diameter in the transition regime, even for nonspherical and agglomerate particles (Rogak et al. 1993; Chakrabarty et al. 2008). The TEM volume distribution was based on the assumption of spherical particles.

The limitations of Silicone TEM images outlined above preclude the creation of a reliable size distribution by microscopy, and the fractal nature of Teflon particles does not give size distribution statistics, which are directly comparable with spherical aerosols, thus only Kapton, lamp wick, and Pyrell were analyzed. TEM size distributions for Pyrell appear in the SI. Size distributions of a typical high temperature Kapton test are shown in Figure 4a. The unaged smoke has $d_g = 158$ nm and $\sigma_g = 1.68$, and after 12 minutes of aging, d_g increases to 210 nm and σ_g shrinks to 1.63. This supports observations on Figure 3a, which shows aged particles with a narrower size range and uniformly larger diameters.

A TEM lamp wick particle size distribution of particles collected during ground testing is compared with SMPS results in Figure 4b. Two different smoke tests are compared but the heating temperatures are within 0.6°C, so the pyrolysis can be

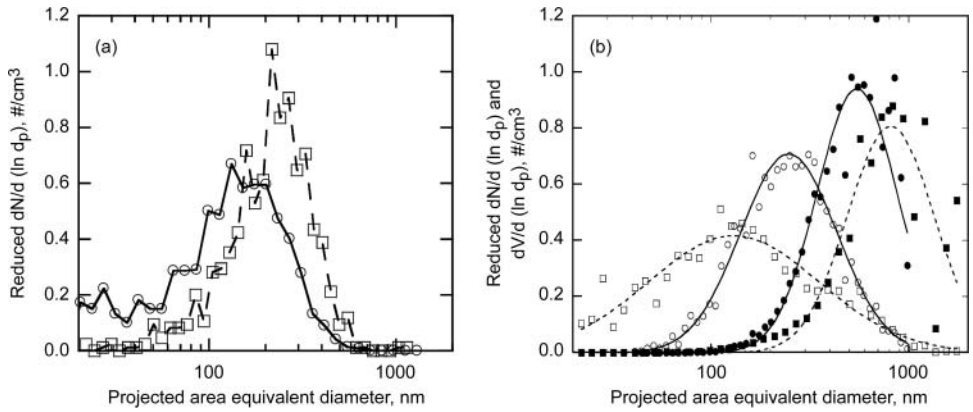

FIG. 4. TEM particle size distributions for Kapton and lamp wick based on projected area equivalent diameters. (a) The effect of aging is shown for a high-temperature Kapton ISS experiment (574°C), circles are unaged smoke, and squares are aged smoke. (b) Ground test number and volume distribution for lamp wick aged test (286°C) from SMPS (circle symbols) and TEM (square symbols). The open symbols are number distribution, and closed ones are volume distribution. Best fit parameters for SMPS are $d_{gn} = 248$ nm, $d_{gv} = 548$ nm, $\sigma_{gn} = 1.75$ and $\sigma_{gv} = 1.59$, and for TEM are $d_{gn} = 123$ nm, $d_{gv} = 812$ nm, $\sigma_{gn} = 2.70$, and $\sigma_{gv} = 1.65$.

considered to be similar. For TEM analysis, 17 images containing 4668 particles were processed. TEM images displayed two types of particles: dark, high contrast particles and smaller, lower contrast particles. The faint particles could be an artifact on the TEM grid or be the result of poor image quality. Another explanation could be a secondary particle formation event from the pyrolysis products. For this size distribution analysis, all particles were counted without thresholding, so the small faint particles were included in the total, which reduced the geometric mean diameter and caused σ_{gn} to be significantly larger than the SMPS results. The SMPS and TEM volume distributions have a similar spread but do not agree well in the peak location. The largest size bin of this TEM analysis had 12 particles, which is considered statistically significant for this type of analysis (Hinds 1999). The SMPS size distribution ends at 1000 nm, but there is no upper size limit for particles in the TEM size distribution. Additional TEM size distribution results from ISS flight tests are tabulated in the SI.

DISCUSSION

Limitations of Aerosol Instrument Measurement Ranges

Calibration of SAME instruments (described in the SI) was intended to empirically account for differences in the ranges of the instruments. In the ground validation tests, however, the truncated distribution formula (Equation (5)) can shed light on the limitations and uncertainty of the SMPS measurement range for the fuels tested. Particularly when the particle size distributions are converted to surface area or volume distributions, the percentage of the distribution that is lacking can be significant. Furthermore, the upper end of the SMPS size distribution measurement may not be as reliable because it can be affected by poor counting statistics and these bins are more susceptible to multiple charge correction errors. Therefore, it is prudent to compare a more conservative upper SMPS limit of 700 nm along with a full recorded range to 1000 nm, to see the effect of the SMPS measurement range. Thus, if we were to consider the SMPS data to be most reliable one (having the least uncertainty) in the range of 23 to 700 nm, then the truncated distribution formula for $M_{p,\mathrm{rel}}$ can indicate what percentage of the distribution would be captured with this limitation. Figure 5 shows the percentage of the distribution captured by SMPS for two example materials, Kapton and silicone. Kapton is the best candidate for SMPS validation, as the highest percentages of each type of distribution are within the SMPS measurement range. For example, considering both the conservative 700-nm limit and the 1000-nm limit, the bar graph indicates that 98 to 100% of the distribution has been measured. Silicone smoke is not a good candidate for SMPS validation because of the lack of measurement range, particularly when converting to surface and volume size distributions. Notably in the volume distribution in Figure 5b, the black bar representing a 1000-nm upper size limit is only at 40%, indicating that 60% of the distribution is missed by the instrument, but when losses are considered and a range of 700 nm is relied upon, approximately 20% of the distribution is captured (the white bar).

Thus, the truncated distribution formula for $M_{p,\mathrm{rel}}$ can be a useful indicator of the suitability of an aerosol reference instrument and the level of uncertainty in measurements. If enough of the size distribution is known to obtain parameters for a lognormal fit from curve-fitting software, one can determine how comprehensive the size distribution measurement is, and whether conversion of the distribution will produce reliable results.

Comparison of SMPS Data, Discretely Calculated Moment Diameters versus Hatch–Choate Diameters Based on Lognormal Fit Parameters

A useful quantitative measure of the validity of the lognormal assumption is to start with one set of data and compare diameters calculated by two different methods. The SMPS data offer the opportunity to use grouped data discretely, and based on the lognormal fit values of d_g and σ_g, the same diameters can be calculated with the Hatch–Choate equations.

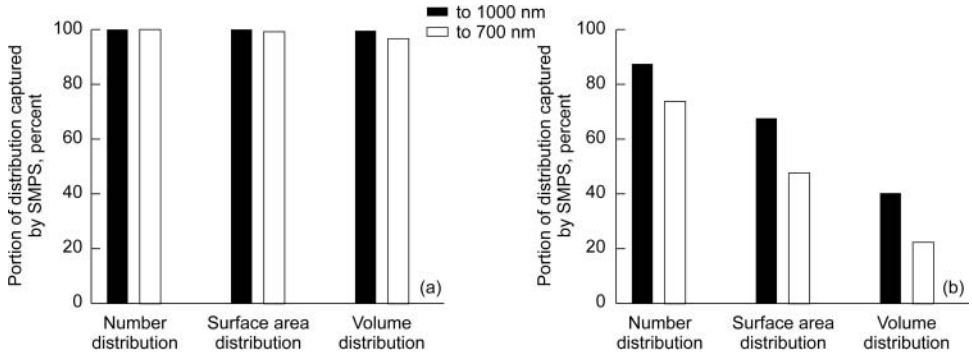

FIG. 5. The percentage of the number, surface area, and volume particle size distributions captured by the SMPS (ground testing) for (a) low-temperature (511°C) unaged Kapton smoke, and (b) high-temperature (370°C) unaged silicone smoke. Black bars represent an SMPS upper limit of 1000 nm (as measured) and white bars represent a more conservative upper limit of 700 nm.

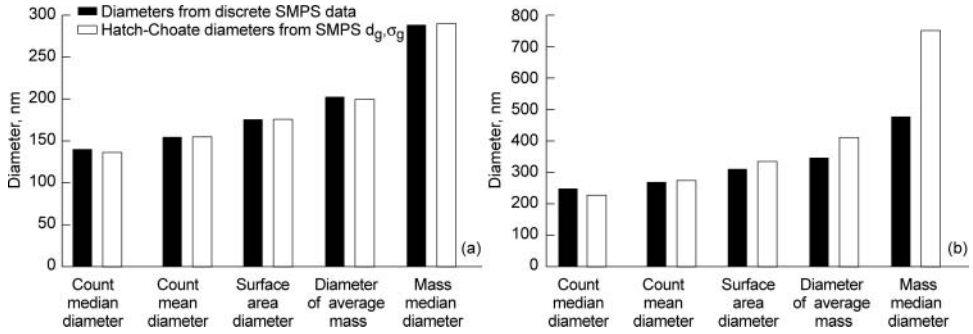

FIG. 6. Two examples of the comparison of diameters calculated from SMPS data (ground testing) in two ways: (1) calculated using discrete SMPS bin data (black bars), and (2) converted by the Hatch–Choate conversion equations using SMPS d_g and σg (white bars) for (a) low-temperature, unaged Kapton smoke, and (b) low-temperature, unaged silicone smoke.

The SMPS bin data (based on a 64-channel per size decade histogram) can be used in Equation (4) formulas to calculate diameters of average properties, which can then be compared with diameters calculated from Equation (3) using the geometric mean diameter and σ_g from the lognormal fit of the SMPS particle size distribution. This is equivalent to calculating N_{tot}, L_{tot}, and M_{tot} from SMPS binned data to obtain d_{av} and d_m, by Equations (1) and (2). Thus, the continuous distribution parameters used in the conversion equations will be compared with the grouped data, and the expectation is that these diameters will be equal if the lognormal assumption is valid. Two examples of these diameter comparisons are shown in Figure 6, which compares the count mean diameter (also known as the number average, or d_{50} of the number distribution), surface area diameter, diameter of average mass, mass median diameter (d_{50} of the volume distribution), and the count median diameter (which is the geometric mean diameter, provided that the distribution is lognormal). As can be seen, there is a good agreement in all diameters for Kapton (Figure 6a) but not as good agreement for silicone (Figure 6b). The diameters with the largest deviations are those having to do with the mass. This is not surprising, since these are heavily influenced by the large diameter particles, and often the SMPS raw counts in the upper bins of the tail have fewer than 10 particles, so there is a potential for discrepancies in discrete bin calculations due to insufficient statistics.

Figure 7a shows the results of all bar graphs from comparison of the three spherical aerosols on one plot (including unaged and aged diameters, at all temperatures tested). The black bars of Figure 6 are the y-axis quantity in Figure 7a and the white bars are the x-axis quantity. Data falling on the 1:1 reference line meet the lognormal assumption, whereas those that differ significantly do not. While some information is lost in this scatter plot versus the bar graphs (e.g., which data marker represents which moment diameter), the graph shows that for Kapton and lamp wick, the diameters calculated by both methods coincide and thus can be considered lognormal. It is evident that diameters above 500 nm, which are the higher

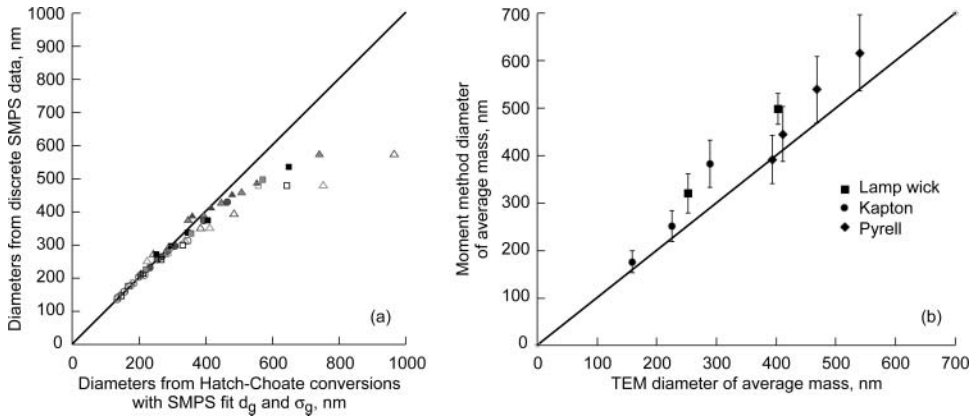

FIG. 7. Comparison of moment method diameters by different techniques. (a) Ground testing diameters calculated from SMPS data in two ways: converted by the Hatch–Choate conversion equations using SMPS lognormal fit d_g and σg plotted against diameters calculated using discrete SMPS bin data. All diameters analyzed as in Figure 6 are combined here for all materials and test conditions: open markers are unaged, solid are aged; gray represents baseline temperature, black represents high temperature tests, and marker shapes are Kapton: circle, lamp wick: square, and silicone: triangle. (b) ISS flight data comparison of diameter of average mass by TEM analysis and the moment method.

moment diameters, and mostly silicone, do not coincide. Overall, the qualitative comparison of these diameters strongly suggests that the smoke particle size distributions for Kapton® and lamp wick can be considered lognormal and silicone should not.

Comparison of Size Distribution Parameters from TEM and Moment Method Measurements from Flight Data

Although meticulous calibrations were performed, a number of smoke aerosols measured in flight tests exceeded the calibration range of ionization detector which measures the first moment. As evident in the uncertainty analysis (see the SI), error in the first moment measurement has the largest influence on the resulting calculations. Kapton consists of smaller particles and was not affected by this shortcoming, so these tests provided the most reliable moment method results. Since the first moment measurement is not used in the calculation of d_m, this quantity can be compared for other materials.

Figure 7b shows the comparison of the flight TEM diameter of average mass with the value calculated from the moment instrument data using Equation (2). Since the third moment instrument was calibrated for each smoke type with a direct-reading reference instrument, the measurements are assumed to be relatively shape-independent (see the SI). For the three materials in this graph, the moment method provides a reasonably good measurement for the diameter of average mass. Thus, it can be concluded that the zeroth and third moment instruments maintained their calibration sufficiently to quantify this moment average diameter from flight data.

CONCLUSIONS

The aerosols considered in SAME represent the most likely smokes that a spacecraft fire detector will have to detect. We have characterized these smoke aerosols, and conclude with the following observations:

1. TEM analysis of the particles from five spacecraft revealed distinct morphologies ranging from nearly spherical (Kapton and lamp wick) to extended aggregates (Pyrell and Teflon).
2. The silicone particles were not stable enough for TEM analysis.
3. Successful size distributions from TEM analysis were obtained for the more spherical particles (Kapton and lamp wick), as well as for Pyrell, as the projected area-equivalent diameter is comparable with mobility diameter, even for nonspherical particles.
4. SMPS measurements were made for all five materials.
5. Comparison of SMPS and TEM size distribution measurements showed reasonable but not complete agreement.
6. Comparison of TEM and moment measurement results from the space experiments showed good agreement for the three materials whose morphology was amenable to TEM analysis (Kapton, Pyrell, and lamp wick).
7. Statistical analysis of SMPS measurements showed that the spherical particles, Kapton and lamp wick, can be characterized as lognormal.
8. Although a direct comparison of TEM, SMPS, and moment instrument results was not possible, the observed sizes from each system were quite consistent, given the constraints of each measurement type.

The moment method for the measurement of size distribution parameters relies on two assumptions: spherical particles and a lognormal distribution. These conditions were reasonably met in two of the five materials tested (Kapton and lamp wick). However, using the output from the calibrated SAME moment instruments, one is able to partially characterize the aerosol by determining d_m and d_{av} for any particle morphology. Within the limitations of spacecraft fire detection, the moment method was considered as a candidate for smoke aerosol measurement and has been proved moderately effective.

The smokes observed for these spacecraft materials cover a broad range in particle size. Ambient aerosols in spacecraft include significantly larger particles than on the Earth, as gravitational settling is absent, and smoke detectors must distinguish between background aerosols and smoke in order to prevent false alarms. Therefore, the typical background aerosols in manned spacecraft should be characterized and taken into account for smoke detector designs. Spacecraft fire detection systems require years of maintenance-free operation. This will be an important challenge for future longer-term space missions, as the expertise and resources necessary to calibrate and/or repair aerosol instruments in flight would not be available.

ACKNOWLEDGMENTS

The SAME experiment team and the crews of ISS increments 10, 13, 15, and 24 are gratefully acknowledged. The SAME project was conducted through the ISS Exploration Research Project of the Exploration Technology Development Program.

SUPPLEMENTAL MATERIAL

Supplemental material for this article can be accessed on the publisher's website.

REFERENCES

Brooker, J. E., Urban, D. L., and Ruff, G. A. (2007). ISS Destiny Laboratory Smoke Detection Model, *International Conference on Environmental Systems*, *07ICES-113, 2007*, Chicago, IL.

Bukowski, R. W., and Mulholland, G. W. (1978). *Smoke Detector Design and Smoke Properties*, NBS Technical Note 973. National Bureau of Standards, Washington, DC.

Bukowski, R. W., Peacock, R. D., Averill, J. D., Cleary, T. G., Bryner, N. P., Walton, W. D., Reneke, P. A., and Kuligowski, E. D. (2003). Performance of Home Smoke Alarms, Analysis of the Response of Several Available Technologies in Residential Fire Settings, NIST Technical Note 1455, December 2003.

Chakrabarty, R. K., Moosmüller, H., Chen, L.-W. A., Lewis, K. A., Arnott, W. P., Mazzoleni, C., Dubey, M. K., Wold, C. E., Hao, W. M., Kreidenweis, S. M. (2010). Brown Carbon in Tar Balls from Smoldering Biomass Combustion. *Atmos. Chem. Phys.* 10:6363–6370.

Chakrabarty, R. K., Moosmüller, H., Garro, M. A., Arnott, W. P., Slowik, J. G., Cross, E. S., Han, J.-H., Davidovits, P., Onasch, T. B., and Worsnop, D. R. (2008). Morphology-Based Particle Segregation by Electrostatic Charge. *J. Aerosol Sci.* 39:785–792.

Chen, B. T., Namenyi, J., Yeh, H. C., Mauderly, J. L., and Cuddihy, R. G. (1990). Physical Characterization of Cigarette Smoke Aerosol Generated from a Walton Smoke Machine. *Aerosol Sci. Technol.* 12 (2):364–375.

Cleary, T. G., Weinert, D. W., and Mulholland, G. W. (2003). *Moment Method for Obtaining Particle Size Measures of Test Smokes*, NISTIR 7050. National Institute of Standards and Technology, Gaithersburg, MD.

Hinds, W. C. (1999). *Aerosol Technology*, 2nd Ed.. Wiley Interscience, New York, NY.

Janhäll, S., Andreae, M. O., and Pöschl, U. (2010). Biomass Burning Aerosol Emissions from Vegetation Fires: Particle Number and Mass Emission Factors and Size Distributions. *Atmos. Chem. Phys.* 10:1427–1439.

Li, W., and Hopke, P. K. (1993). Initial Size Distributions and Hygroscopicity of Indoor Combustion Aerosol Particles. *Aerosol Sci. Technol.* 19:305–316.

Mack, L. A., Levin, E. J. T., Kreidenweis, S. M., Obrist, D., Moosmüller, H., Lewis, K. A., Arnott, W. P., McMeeking, G. R., Sullivan, A. P., Wold, C. E., Hao, W. M., Collett Jr., J. L., Malm, W. C. (2010). Optical Closure Experiments for Biomass Smoke Aerosols. *Atmos. Chem. Phys.* 10: 9017–9026.

Maricq, M. M. (2013). Monitoring Motor Vehicle PM Emissions: An Evaluation of Three Portable Low-Cost Aerosol Instruments. *Aerosol Sci. Technol.* 47(5–7):564–573.

Moosmüller, H., Arnott, W. P., Rogers, C. F., Bowen, J. L., Gillies, J. A., Pierson, W. R., Collins, J. F., Durbin, T. D., Norbeck, J. M. (2001). Time-Resolved Characterization of Diesel Particulate Emissions. 1. Instruments for Particle Mass Measurements. *Environ. Sci. Technol.* 35:781–787.

Mulholland, G. W. (1995). Smoke Production and Properties, in *SFPE Handbook of Fire*, 2nd Edition, DiNenno, P. J., Beyler, R. L., Custer, P., Walton, W. D., Watts, J. C. L. M., Drysdale, D., and Hall, J. R., eds., Society of Fire Protection Engineers, Boston, Mass., pp. 2-217–2-227.

Mulholland, G. W., Meyer, M., Urban, D. L., Ruff, G. A., Yuan, Z., Bryg, V., Cleary, T., and Yang, J. (2015). Pyrolysis Smoke Generated under Low-Gravity Conditions, *Aerosol Sci. Tech.* 49(5):310–321.

Raabe, O. G. (1971). Particle Size Analysis Utilizing Grouped Data and the Lognormal Distribution. *J. Aerosol Sci.* 2:289–303.

Reist, P. C. (1984). *Introduction to Aerosol Science*. Macmillan, New York, NY.

Rogak, S. N., Flagan, R. C., and Nguyen, H. V. (1993). The Mobility and Structure of Aerosol Agglomerates. *Aerosol Sci. Technol.* 18:25–47.

Xie, Q., Yuan, H., Song, L., and Zhang, Y. (2007). Experimental Studies on Time-Dependent Size Distributions of Smoke Particles of Standard Test Fires. *Build. Environ.* 42:640–646.

Zai, S., Zhen, H., and Jia-Song, W. (2006). Studies on the Size Distribution, Number and Mass Emission Factors of Candle Particles Characterized by Modes of Burning. *J. Aerosol Sci.* 37:1484–1496.

Supplemental Information

Smoke Characterization and Feasibility of the Moment Method for Spacecraft Fire Detection

Marit Meyer,[1] George W. Mulholland,[2,3] Victoria Bryg,[4] David L. Urban,[1] Zeng-guang Yuan,[4] Gary A. Ruff,[1] Thomas Cleary,[3] and Jiann Yang[3]

[1] *NASA Glenn Research Center, Cleveland, OH, USA*
[2] *University of Maryland, College Park, MD, USA*
[3] *National Institute of Standards and Technology, Gaithersburg, MD, USA*
[4] *National Center for Space Exploration Research, Cleveland, OH, USA*

SAME Instrument Calibration

An in-depth empirical calibration of the moment instruments was performed on the ground before the flight experiments. Calibration of the moment instruments used in SAME was essential to properly interpret the flight data and was performed on the ground before the flight. Calibration was accomplished using two different aerosol generators: one using mono-disperse particle generation using dioctyl phthalate (DOP) according to the approach by Mulholland and Liu (1980) and the other using polystyrene spheres. The aerosol from the generator was sampled simultaneously by the SAME instrument under test and a reference instrument. For the number count, the reference instrument was a condensation particle counter[1] (CPC 3022A, TSI, Shoreview, MN, USA) (Fletcher et al. 2009), for the mass concentration, a tapered element oscillating microbalance (TEOM, Thermo Scientific, Franklin, MA, USA) and for the first moment an electrical aerosol detector (EAD, 3070A, TSI, Shoreview, MN, USA) was used. The results for the P-Trak™ calibration are shown in Fig. S1. As the number concentration increased, the effect of the particle diameter became more evident. Separate correlations were developed for each particle size and the closest correlation was used to analyze the flight data based on the initial estimates of the average particle size.

P-Trak™ hardware changes to adapt the commercial off the shelf instrument for low gravity were tested in a separate space experiment with good results indicating the modifications to the device were successful. A wide range of dilution was required for the different smoke aerosols generated, so a device called a Dynamic Diluter was developed to ensure the P-Trak™ would not saturate. It consists of a proportional-integral-derivative (PID) controller, a servo valve that controls the flow rate of the diluting nitrogen gas, and a laminar flow element (LFE) for the aerosol stream. The controller reads the desired dilution ratio from the software (based on the sample material to be heated) and the pressure drop over the LFE. The controller output voltage to the servo valve controls the nitrogen flow for dilution upstream of the P-Trak.™ The PID control principle ensures that the actual dilution ratio matches the desired dilution ratio commanded by the software. Aerosol flow through the LFE ranged from 1 to 120 sccm, where the balance of the 700 sccm P-Trak™ flow rate was nitrogen.

[1] ***Certain commercial equipment, instruments, or materials are identified in this paper to foster understanding. Such identification does not imply recommendation or endorsement by the National Aeronautics and Space Administration or the National Institute of Standards and Technology, nor does it imply that the materials or equipment identified are necessarily the best available for the purpose.***

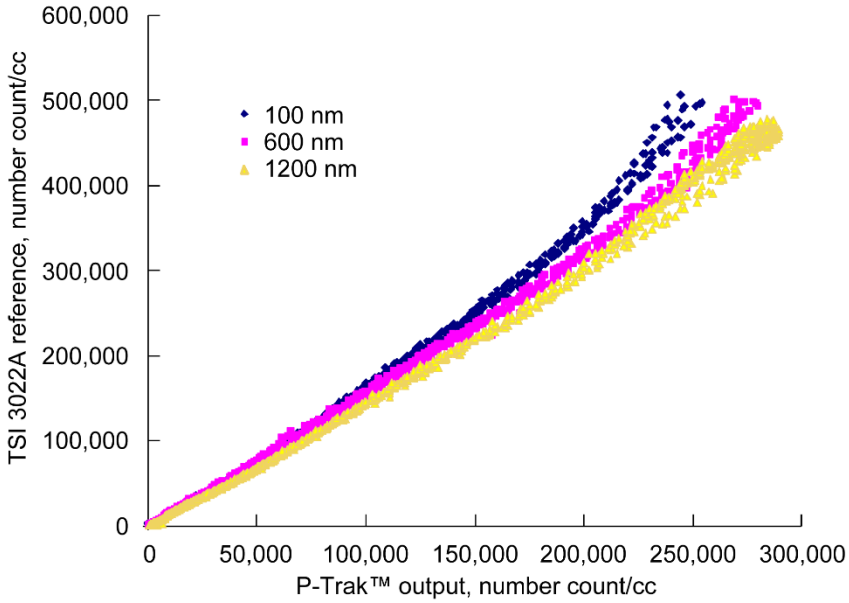

FIG. S1. P-Trak™ Calibration results with three sizes of monodisperse DOP droplets, CPC concentration plotted against P-Trak™ concentration.

The first moment device, the ionization chamber, showed little effect of particle size as seen in Fig S2. Consequently a single correlation was used for all particle sizes. The third moment device (DustTrak™) has a response which varies with the particle refractive index. This issue was addressed by calibrating the DustTrak™ with the smoke aerosol from each material. In the results reported here, the DustTrak™ response was directly calibrated, for each smoke source, against mass concentration measurements using a tapered element oscillating microbalance. These 1-g calibrations are assumed to be valid in low gravity.

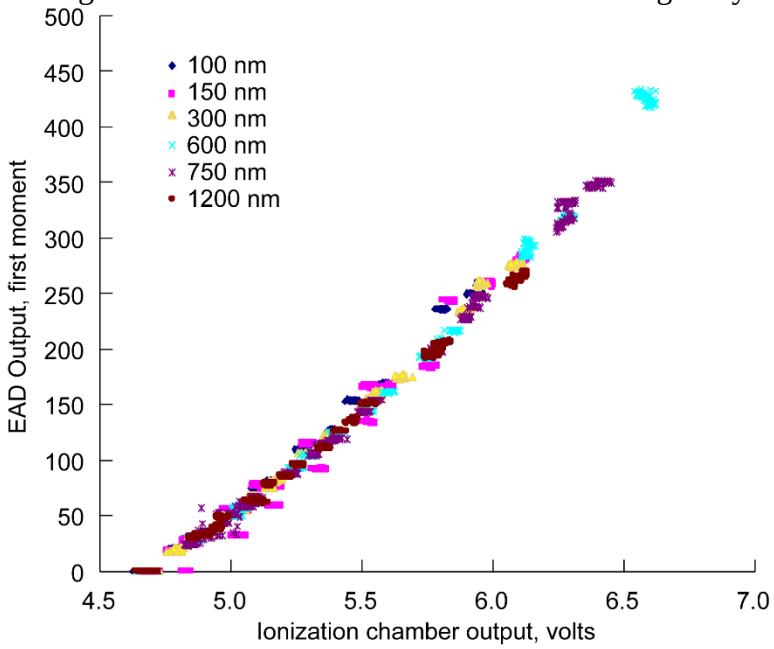

FIG. S2. Ionization Chamber Calibration results with monodisperse DOP droplets.

Thermal Precipitator Design

The thermal precipitator posed a unique engineering challenge, in that crew members receive minimal training in the experiment procedure, often up to a year in advance of the actual flight. Hardware must be relatively simple to install, with a minimum number of larger integrated components, as small objects can escape in microgravity and are hard to retrieve. The design approach was to make interchangeable grid-containing units with a software controlled flow manifold allowing smoke particle deposition on twelve TEM grids (one grid per test point). A detail of the flow path through one half of the thermal precipitator is shown in Figure S3, and the fully assembled unit is shown in Figures S4 and S5. A total of six thermal precipitator units were launched for this experiment, providing a potential of 72 TEM grids for analysis. Unfortunately, approximately half of the data was lost owing to malfunctioning of the flow in the manifold. The Kanthal wire is oriented above the TEM grid and particles deposit uniformly slightly downstream of the wire, after the particle enters the region of the thermal gradient. Figure S5 shows the deposition boundary of the particles, and images used for size distribution analysis by microscopy were taken only beyond the deposition boundary. The TEM size distributions were constructed by first locating the downstream edge of the particle deposition. Sequential images were then taken by traversing the grid in a line moving from one edge of the aerosol deposition to the other. This protocol was repeated until a large number of particles were counted. Images were processed to remove any background and adjusted to high contrast before setting a threshold. The TEM particle size analysis method used ImageJ, an open source, public domain image processing progam (Rasband, W.S., ImageJ, U. S. National Institutes of Health, Bethesda, Maryland, USA, http://imagej.nih.gov/ij/, 1997-2012). The TEM grids were examined with a Philips™ CM20 Transmission Electron Microscope at 200KV and images were collected using an Olympus™ Veleta camera. The digital camera was calibrated using a MAG*I*CAL® calibration reference which is a NIST traceable standard.

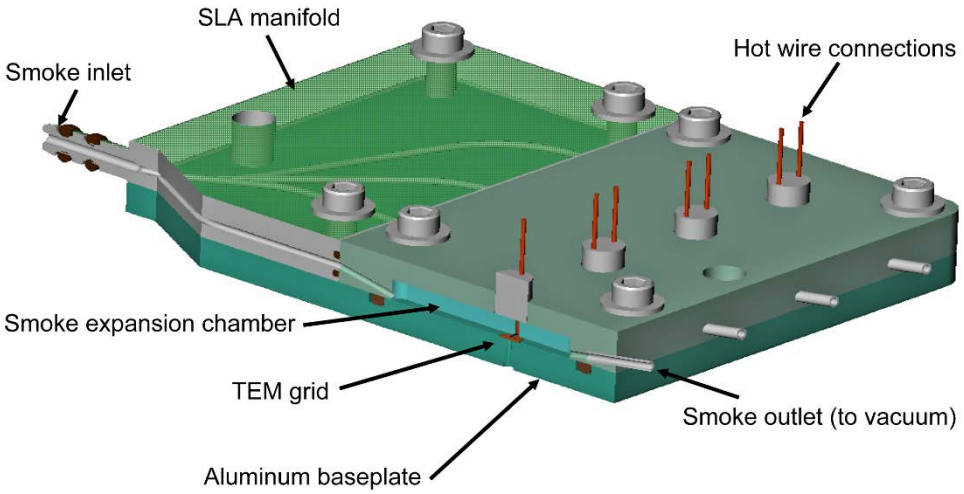

FIG. S3. A cut-away view of one side of a Thermal Precipitator Unit with the inlet manifold exposed on the left, the hot wire leads in the center block and the outlet valves on the right. The manifold was 3D printed using stereolithography (SLA).

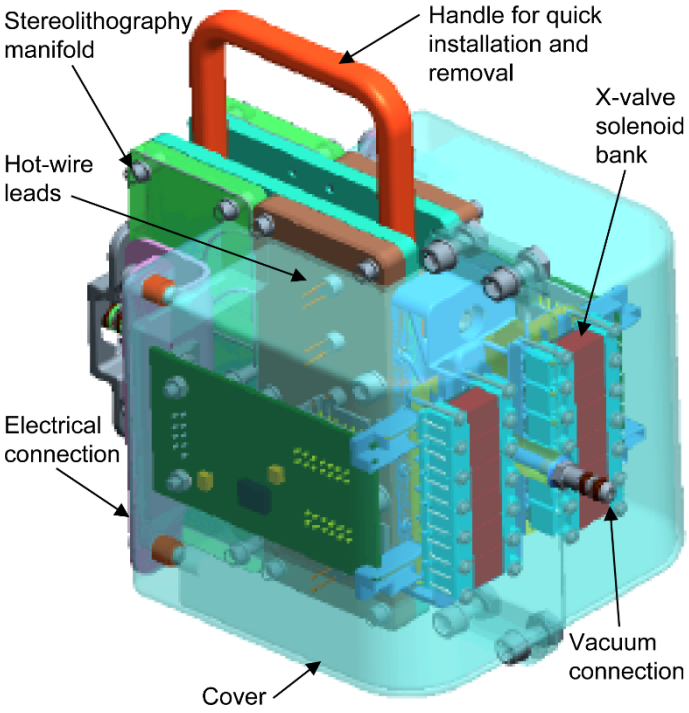

FIG. S4**.** Fully assembled thermal precipitator which has a total of 12 TEM grids, 6 on each side.

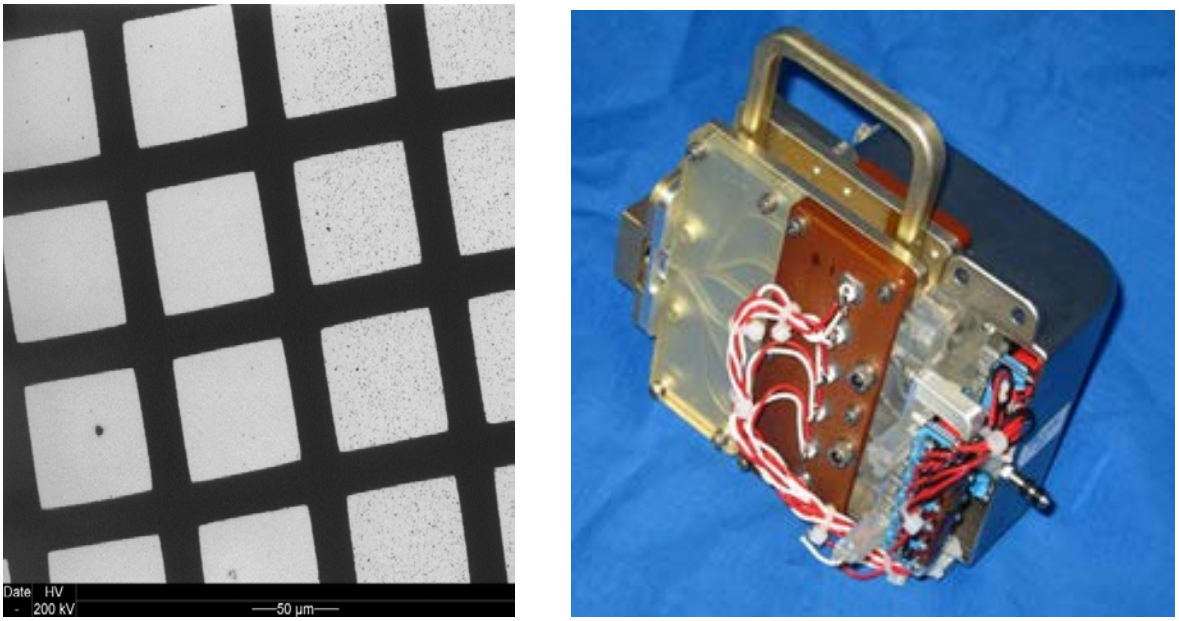

FIG. S5. TEM grid showing the deposition boundary of particles (left image), and the thermal precipitator unit with circuit card and cover removed for detail (right image).

Moment Method Overview

Three moments of the smoke particle size distribution (zeroth, first, and third) were measured, and using the properties of the lognormal distribution, the geometric mean diameter and the standard deviation of the aerosol were calculated. Two assumptions are made when using this method: the aerosol particles maintain a spherical (or nearly-spherical) shape and the size distribution is lognormal.

We provide a detailed overview of the moment method here in the online supplemental information. The average particle size and the width of the size distribution are estimated from various moments of the size distribution. The number distribution, n_d, is defined as

$$n_d = \frac{dN(d_p)}{d(d_p)} \tag{S1}$$

where $dN(d_p)$ is the number of particles per cm^3 with diameter between d_p and $d_p + d\,d_p$. The moments of interest in SAME are the zero-th moment, first and third moments, denoted by M_0, M_1 and M_3 below respectively. They are defined as

$$M_i \equiv \int_0^\infty d_p{}^i n_d d(d_p), \quad \text{i} = 0, 1, 2, 3 \ldots \tag{S2}$$

The zero-th moment is equal to the total number concentration, N_{tot}. When particles can be characterized as spherical, first moment is equal to the total diameter length concentration, or the integrated diameter per unit volume, L_{tot}, and the 3rd moment is proportional to the total volume and/or mass concentration ($M_{tot} = \pi\rho M_3/6$) which includes the particle density.

Thus, one can obtain the commonly used count mean diameter (simple average), d_{av}, and the diameter of average mass, d_m

$$d_{av} = \left(\frac{M_1}{M_0}\right) = \frac{L_{tot}}{N_{tot}} \qquad d_m = \left(\frac{M_3}{M_0}\right)^{1/3} = \left(\frac{6M_{tot}}{\pi\rho N_{tot}}\right)^{1/3} \tag{S3,S4}$$

Equations (S3) and (S4) are special cases of the general expression for the *p-th* moment average of the q-th moment distribution, $d_{p,q}$ which is as follows:

$$d_{p,q} = \left(\frac{\int_0^\infty n_d d_p^{\,p} d_p^{\,q} d(d_p)}{\int_0^\infty n_d d_p^{\,q} d(d_p)}\right)^{1/p} \tag{S5}$$

Thus, from three measured data, N_{tot}, L_{tot} and M_{tot} we obtain the diameters d_{av}, and d_m, regardless of what form the particle size distribution exhibits.

The determination of d_{av} is independent of shape and calculating d_m requires only that the three dimensions of a particle are isometric (ie. not fractal agglomerates). There is no assumption about the form of the size distribution. However, to determine the geometric standard deviation, σ_g, of the size distribution, or other moment diameters by the moment method requires that the size distribution be lognormal. The lognormal distribution is widely used for describing aerosols including non-flaming smoke because for most smoke aerosols, the bulk of the number concentration is associated with smaller particles (Raabe 1971; Reist 1984). Many studies have assumed that pyrolysis and combustion smoke aerosols from various fuels have a lognormal size distribution (Chen et al. 1990; Li and Hopke 1993; Zai et al. 2006; Xie et al. 2007; Janhäll et al. 2010; Chakrabarty et al. 2010; Mack et al. 2010).

If ln d_p, instead of d_p, is used as the independent variable in a lognormal distribution, the distribution becomes a normal distribution function. In other words, the lognormal distribution with respect to d_p is a normal distribution with respect to ln d_p. The advantage of converting a lognormal distribution to a normal distribution by using ln d_p as the independent variable is that the peak location is unchanged for a fixed geometric mean diameter, d_{gn}, as the geometric standard deviation, σ_g, varies. Furthermore, the widths of the number and volume distributions are the same when ln d_p is plotted as the x-variable, that is, the geometric standard deviation is equal for both distributions. Symmetry of a distribution, when plotted with ln d_p as the independent variable is an indication that the distribution is lognormal.

The normal distribution with ln d_p as the independent variable has the following form:

$$n_1(\ln d_p) = \frac{dN(d_p)}{d\ln d_p} = \frac{N_{tot}}{\sqrt{2\pi}\ln\sigma_{gn}}\exp\left[-\frac{(\ln d_p - \ln d_{gn})^2}{2(\ln^2\sigma_{gn})}\right] \qquad \text{(S6)}$$

where the subscript n in d_{gn} and σ_{gn} indicate that the geometric mean diameter and geometric standard deviation are based on the number size distribution and N_{tot} is the total number concentration of the aerosol (= M_0). Similarly, a geometric mean diameter of the particle volume distribution is d_{gv}, with a corresponding geometric standard deviation for the volume distribution being denoted as σ_{gv}. The geometric standard deviation, σ_{gn} is the standard deviation of the logarithms of the particle diameters. The geometric mean diameter and geometric standard deviation are defined in the same way as for a normal distribution except in the formulas, d_p is replaced with the *ln* d_p.

$$\ln d_{gn} = \frac{\sum n_i \ln d_i}{N} \qquad \ln^2\sigma_{gn} = \frac{\sum n_i(\ln d_i - \ln d_{gn})^2}{N-1} \qquad \text{(S7,S8)}$$

Formulas (S1) through (S5) are valid for any particle size distribution. However, if the particle size distribution is lognormal, then σ_{gn}, σ_{gv}, σ_g are all the same and the Hatch-Choate conversion equations (Hinds, 1999) can be used to calculate many different average diameters if d_{gn}, and one σ is known (Raabe 1971; Reist 1984). The general formula for the *p*th moment average of the *q*th moment distribution is

$$d_{p,q} = d_{gn} \exp\left[(q + \frac{p}{2}) \ln^2 \sigma_g \right] \quad \text{(S9)}$$

where σ_g is the same for particle number and volume distributions and d_{gn} is equal to the count median diameter of the distribution due to the lognormal assumption. For converting to the count mean diameter, d_{av} (= $d_{1,0}$) and the diameter of average mass, d_m (= $d_{3,0}$) the corresponding values of $(q+p/2)$ are 0.5 and 1.5. Using the two diameters d_{av} and d_m we obtain from the moment instruments in the general equation (S9), we get the following explicit equations to calculate the parameters of the lognormal distribution:

$$\sigma_g = \exp\sqrt{\ln(d_m / d_{av})} \qquad d_{gn} = \sqrt{d_{av}{}^3 / d_m} \quad \text{(S10,S11)}$$

Note that σ_g can be calculated when any pair of the three diameters d_{gn}, d_{av} and d_m are known. By combining the three moments M_0, M_1 and M_3, it is possible to compute different mean diameters of any smoke particle size distribution, and if the distribution is lognormal, the geometric mean diameter and standard deviation can be calculated as well. Validation of this approach is discussed in Cleary, Weinert and Mulholland (Cleary et al. 2003). This statistical method is currently the best option for estimating the size distribution parameters of a smoke aerosol in low gravity.

If a histogram of particle sizes is available, the diameter of an average property proportional to $(d_p)^p$ can be calculated for i bins with the following formula:

$$d_{\bar{p}} = \left(\frac{\sum n_i d_i{}^p}{N} \right)^{1/p} \quad \text{(S12)}$$

With this formula, binned data from a reference instrument can be used to verify results from moment method calculations.

Aerosol instruments are limited in their measurement ranges, and the accuracy of the measurements may vary over the range as well. If the moments of the particle size distribution are determined by instruments that are not identical in their ranges of particle size measurement, we can quantify the truncated moment value normalized by the total moment value. This relative value indicates how much of an actual signal is captured in the limited detection range of an instrument. The formula for a bounded moment measurement which assesses the uncertainty induced by an instrument omitting particles above or below a certain diameter D is based on the p moment cumulative function of a lognormal distribution with d_g and σ_g. If D is the particle size below which no signal can be detected, the relative cumulative *p-th* moment is

$$M_{p,rel} = \frac{1}{2}[1 + erf(\eta_D)] \qquad \text{where} \qquad \eta_D = \frac{ln\left(\frac{D}{d_g}\right)}{\sqrt{2} ln\sigma_g} - \frac{1}{\sqrt{2}} p ln\sigma_g \quad \text{(S13)}$$

Note that the limiting diameter D is normalized by d_g. This relative cumulative moment function, $M_{p,rel}$ gives the percentage of the *p-th* moment instrument signal that is captured when particles smaller than a diameter, D, cannot be detected, assuming a lognormal distribution with d_g and σ_g. Conversely, when $M_{p,rel}$ is subtracted from 1, it gives the percentage of the instrument

signal that is lost due to lack of instrument range beyond diameter *D*. This diameter, *D*, can be any of the moment average diameters, as the subscript p refers to the type of moment average. This formula is also useful for quantifying the effects of using an impactor with a cutoff diameter *D*.

Derivation of the Relative Cumulative Moment Formula

The *p* moment cumulative function of a lognormal distribution with d_g and σ_g is defined as:

$$M_p(D) = \frac{1}{\sqrt{2\pi} ln\sigma_g} \int_0^D d^{p-1} exp\left(-\frac{(lnd - lnd_g)^2}{2(ln\sigma_g)^2}\right) dd \quad \text{(S14)}$$

Using the following new variables, we can simplify the derivation.

$$A = \frac{1}{\sqrt{2\pi} ln\sigma_g}, \quad B = 2(ln\sigma_g)^2, \quad C = lnd_g \text{ and } L = lnd. \quad \text{(S15)}$$

Thus the simplified form of (S14) is:

$$M_p(D) = A \int_{-\infty}^{lnD} exp\left(pL - \frac{(L-C)^2}{B}\right) dL \quad \text{(S16)}$$

It can be shown that

$$pL - \frac{(L-C)^2}{B} = pC + 0.25p^2B - \frac{1}{B}(L - C - 0.5pB)^2 \quad \text{(S17)}$$

Define two new variables to simplify the derivation:

$$\xi = pC + 0.25p^2B \text{ and } \eta = \frac{L - C - 0.5pB}{\sqrt{B}} \quad \text{(S18)}$$

From (S18), we have that $dL = \sqrt{B} d\eta$

Now, (S16) can be rewritten as

$$M_p(D) = A\sqrt{B} \int_{-\infty}^{\eta_D} \exp(\xi - \eta^2)\, d\eta = A\sqrt{B} \exp(\xi) \int_{-\infty}^{\eta_D} \exp(-\eta^2)\, d\eta \quad \text{(S19)}$$

or, in terms of the error function, we have

$$M_p(D) = \frac{\sqrt{\pi}}{2} A\sqrt{B} exp(\xi)[1 + erf(\eta_D)] \quad \text{(S20)}$$

where $\eta_D = \frac{lnD - C - 0.5pB}{\sqrt{B}} = \frac{ln\left(\frac{D}{d_g}\right)}{\sqrt{2} ln\sigma_g} - \frac{1}{\sqrt{2}} p ln\sigma_g$ (S21)

Next, eliminate all intermediate variables to express $M_p(D)$ in terms of d_g, σ_g and *p*. Equation (S20) can be rewritten as:

$$M_p(D) = \frac{1}{2} d_g^p exp\left(0.5\left(p ln\sigma_g\right)^2\right)[1 + erf(\eta_D)] \quad \text{(S22)}$$

It is interesting to see when *D* approaches infinity, what the total *p* moment is. As *D* approaches infinity, η_D approaches infinity too and the error function approaches 1. Thus, the total *p* moment of the lognormal distribution is

$$M_p = M_p(\infty) = d_g^p exp\left[0.5\left(p ln\sigma_g\right)^2\right] \quad \text{(S23)}$$

Equations (S22) and (S23) are very useful, as they give the absolute value of the *p-th* moment, partial or total. The dimension of the p-th moment is [L^p]. However, in many cases, we are interested in the relative value to the total moment or the moment value normalized by the total *p-th* moment value. The relative values can tell us how much of the signal is captured in the limited detection range of an instrument. Dividing Eq. (S22) by Eq. (S23), we have

$$M_{p,rel} = \frac{1}{2}[1 + erf(\eta_D)] \quad \text{(S24)}$$

The resulting equation (S24) is simple and useful. Note that in equation (S21), D is normalized by d_g. Thus $M_{p,rel}$, the relative cumulative value only depends on three parameters, normalized D, σ_g and p.

Uncertainty Analysis of Moment Method

Errors will be intrinsic in the measured moments and the propagation of error will affect the resulting calculated values of d_g and σ_g.

The mass concentration was measured with the DustTrak with a repeatability uncertainty, $u_{r,repeat}(M_c)$, of 0.03 for mass concentrations above 5 mg/m^3. The DustTrak was calibrated in a series of normal gravity experiments over the same range of heater conditions as used in the low-gravity experiments with a tapered element oscillating microbalance (TEOM). The uncertainty in the average calibration constant, $u_{r,cal}(M_{3,c})$, ranges from a few percent for lamp wick, silicone, and Teflon to about 20 % for Pyrell and Kapton. The uncertainty of the mass calibration of the TEOM, $u_{r,TEOM}(M_{3,c})$, was 0.1. The combined uncertainty for M_c, $u_{r,c}(M_c)$, is the quadrature sum (square root of sum of squares) of the three uncertainties:

$$u_{r,c}(M_{3,c}) = [u_{r,repeat}^2(M_3) + u_{r,cal}^2(M_3) + u_{r,TEOM}^2(M_3)]^{1/2} \quad \text{(S25)}$$

By substituting by M_0, M_1 and M_3 in equations (S3) and (S4) into equations (S10) and (S11), we have

$$d_g = \frac{1}{M_0}\sqrt{\frac{M_1^3}{M_3}} \quad \text{(S26)}$$

and

$$\sigma_g = \exp\left(\sqrt{\ln\left(\frac{M_0^{2/3} M_3^{1/3}}{M_1}\right)}\right) \quad \text{(S27)}$$

By differentiating equations (S26) and (S27), we get

$$\frac{dd_g}{d_g} = -\frac{dM_0}{M_0} + 1.5\frac{dM_1}{M_1} - 0.5\frac{dM_3}{M_3} \quad \text{(S28)}$$

and

$$\frac{d\sigma_g}{\sigma_g} = \frac{1}{\ln(\sigma_g^2)}\left(\frac{2}{3}\frac{dM_0}{M_0} - \frac{dM_1}{M_1} + \frac{1}{3}\frac{dM_3}{M_3}\right) \quad \text{(S29)}$$

Since M_0, M_1 and M_3 are measured independently, their relative uncertainties contribute independently to the errors of d_g and σ_g. Denoting combined relative uncertainty as $u_{r,c}$ we have

$$u_{r,c}(d_g) = \left(u_r^2(M_0) + 2.25u_r^2(M_1) + 0.25u_r^2(M_{3,c})\right)^{1/2} \quad \text{(S30)}$$

and

$$u_{r,c}(\sigma_g) = \frac{1}{2\ln(\sigma_g)}\left(\frac{4}{9}u_r^2(M_0) + u_r{}^2(M_1) + \frac{1}{9}u_r{}^2(M_{3,c})\right)^{1/2} \quad \text{(S31)}$$

It is interesting that both equations (S29) and (S30) show the error of M_3 contributes the least to the errors of D_g and σ_g, whereas that of M_1 contributes the most.

Similarly, for d_{av} and d_m, equations (S3) and (S4) have the following relative uncertainties:

$$u_{r,c}(d_{av}) = \left(u_r^2(M_1) + u_r^2(M_0)\right)^{1/2} \quad \text{(S32)}$$

$$u_{r,c}(d_m) = \frac{1}{3}\left(u_{r,c}^2(M_{3,c}) + u_r^2(M_0) + u_r^2(\rho)\right)^{1/2} \quad \text{(S33)}$$

Drum Hardware and Experimental Process

The two 55 gallon drums were minimally modified for use in the ground-based SMPS experiment as follows: A muffin fan was bolted to the circular drum floor opposite the removable lid. All other modifications were made to the lid, including feed-through adapters for tubing and the electrical fan cord, and mounted HEPA filters through which clean air was provided for purging. A four-way crossover valve allowed the drum to be filled with smoke via

a vacuum pump preceded by a flow-controlling orifice, or allowed the smoke to bypass the drum, which effectively isolated the SAME hardware from high pressure during the drum purging process. Transfer of un-aged smoke into the drum began when the SAME software commanded the valve to open and lowered the piston in the aging chamber causing half of the chamber volume to be expelled (3 liters), with the remainder of the smoke retained in the chamber and allowed to age for 12 minutes. The flow rate into the drum was 1.7 L/min, matching the flow rate of a DustTrak™ instrument which the drums replaced (in the original SAME configuration there were two DustTraks). It took less than 2 minutes to transfer the smoke sample into the drum. Tubing from the SAME hardware to the drums was less than one meter in order to minimize transport losses of smoke particles. Initial calculations from previous SAME data indicated that for all materials, the aerosol concentration in the drum would be less than 2×10^4 particles/cm^3, which is below the rule-of-thumb threshold concentration of 10^6 particles/cm^3. Below this level, coagulation can be neglected since it will occur at a very slow rate (Hinds, 1999). Thus it could be assumed that very little aging took place in the drum during the SMPS measurements of un-aged smoke. The drum concentration was well within the counting range of the SMPS so no additional dilution was required for the measurements. During each SMPS sample, the volume of air removed was between 0.5 % and 1.5 % of the drum volume and a correspondingly small number of particles were removed so the drum aerosol concentration was relatively constant during the measurements. Any make-up air needed during the sampling was drawn in through the HEPA filters on the drum lid. The fan in the drum was used to mix the smoke and prevent stratification which could skew the SMPS measurements. First, a 10:1 sheath-to-aerosol flow ratio was used for three consecutive measurements with high fidelity giving particle sizes up to 660 nm. Three subsequent samples were taken with a flow rate ratio of 5:1, in order to reach the largest measurable SMPS particle size of 1000 nm. Considering that aging increases particle size, the higher flow rate ratio (smaller range) gives results for only a portion of the true aged size distribution for most materials in this experiment. Therefore the larger range is important for measurements in spite of the low resolution. After six SMPS scans at two different flow rates, the drum was purged with a continuous flow of HEPA-filtered house air at approximately 309 kPa-g (45 psig), which was exhausted into a fume hood. An additional P-Trak™ was used to indicate when the drum concentration fell below 30 particles/cm^3, which was considered ‘clean’. One set of SMPS measurements for one smoke sample (both aged and unaged) was accomplished in approximately 30 minutes.

Raw counts for the particle size distributions of the SMPS scans indicate the statistical reliability of the data. Of all the data taken, there are sufficient raw particle counts in the majority of bins, however, when there are less than 10 particles in a bin, the reliability is questionable (Hinds, 1999). This is a problem in the tails of the distribution, and compounded with sampling efficiency and losses of large particles in the system, the large diameter tail is particularly affected. In spite of the lower resolution of the low flow aerosol to sheath flow rate ratio, the number of counts per channel is about twice as large for this condition which results in improved statistics. Thus, data from the lower flow rate ratio scans were used exclusively in the data analysis to reduce the uncertainty in the measurements.

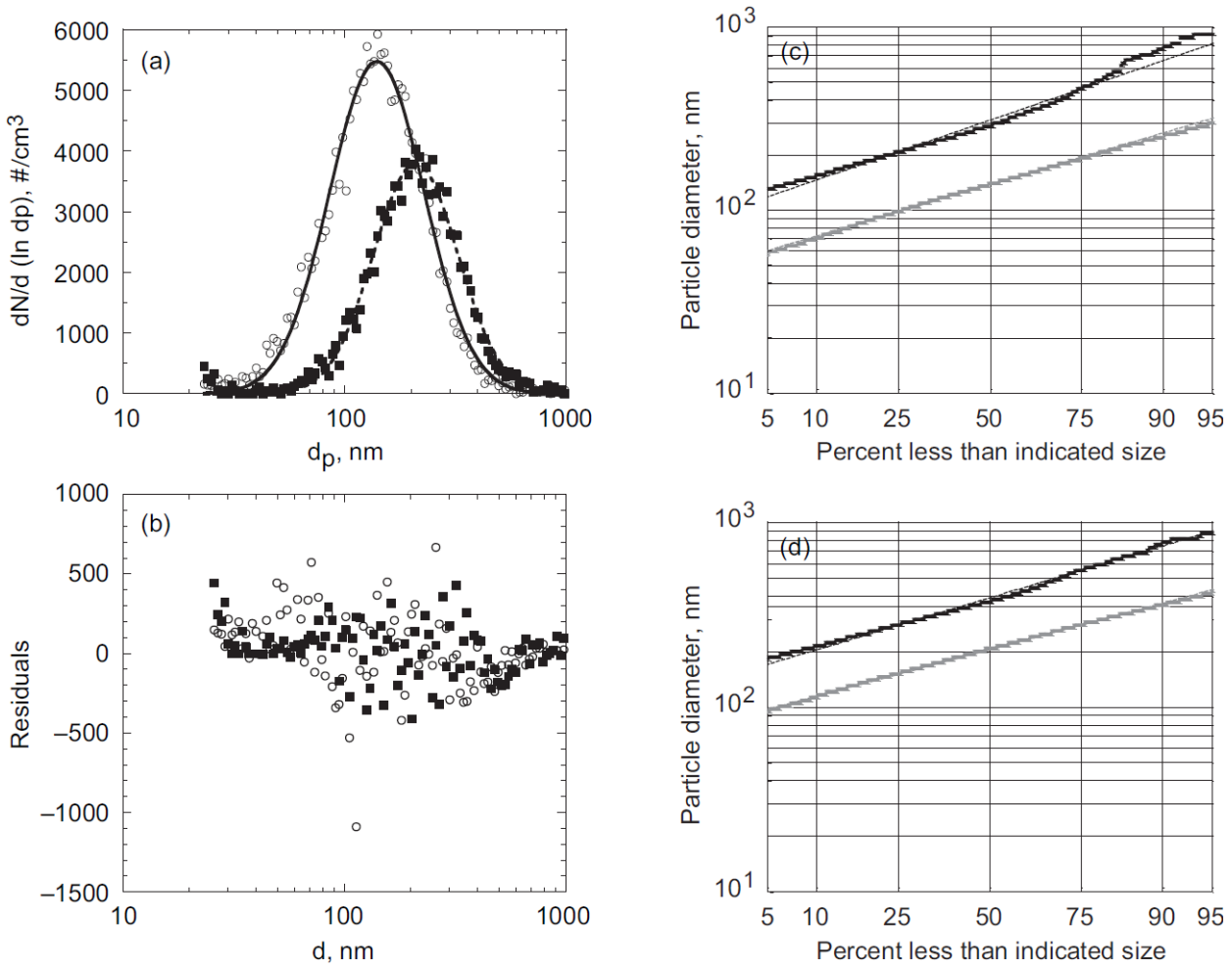

FIG. S6. (a) Smoke particle size distributions from SMPS measurements (ground tests) for a representative Kapton® baseline temperature test (510 °C) with open plot markers for unaged smoke (d_g = 139 nm, σ_g = 1.78) and solid symbols for aged smoke (d_g = 209 nm, σ_g = 1.66). The solid curves represent the non-linear least square fits. (b) A residual plot showing the deviations from the lognormal fits is aligned below the size distribution. Log-probability graphs for unaged (c) and aged (d), based on discrete SMPS bin data. Number distributions are grey, volume distributions are black, and dashed lines are lognormal curve fits.

The log-probability plot is a graphical technique used to assess lognormality of an aerosol. Discrete data from the SMPS size bins are plotted on the probability scale in Figures S6 through S8 parts (c) and (d), corresponding to unaged and aged smoke, respectively. SMPS particle size distributions of the materials are vertically aligned with residual plots in parts (a) and (b) of Figures S6 through S8 for reference and clarity in the discussion of log-probability plots. A lognormal particle size distribution will appear as a straight line on a log-probability graph, and volume and number size distributions should be parallel, indicating that σ_g is the same for both distributions although they have different means. Extremes on the graphs can be neglected in the log-probability plots for number distributions when they deviate from the straight line fit for 5% or less of the extremes of the probability scale (Hinds, 1999). For the SMPS data used in these log-probability plots, these deviations from lognormality are the result

of poor counting statistics in the large diameter tail and lack of measurement range (for lamp wick and silicone), which particularly affects the volume distribution plots. Thus the volume distribution plot will display a line that is slightly curved at the large sizes, which corresponds to a lack of linearity of the number distribution line beyond 95% of the distribution. Figures S6(c) and S6(d) show log-probability plots for Kapton® at baseline temperature. The plotted cumulative frequencies are quite linear for Kapton® and the number and volume distribution lines are nearly parallel.

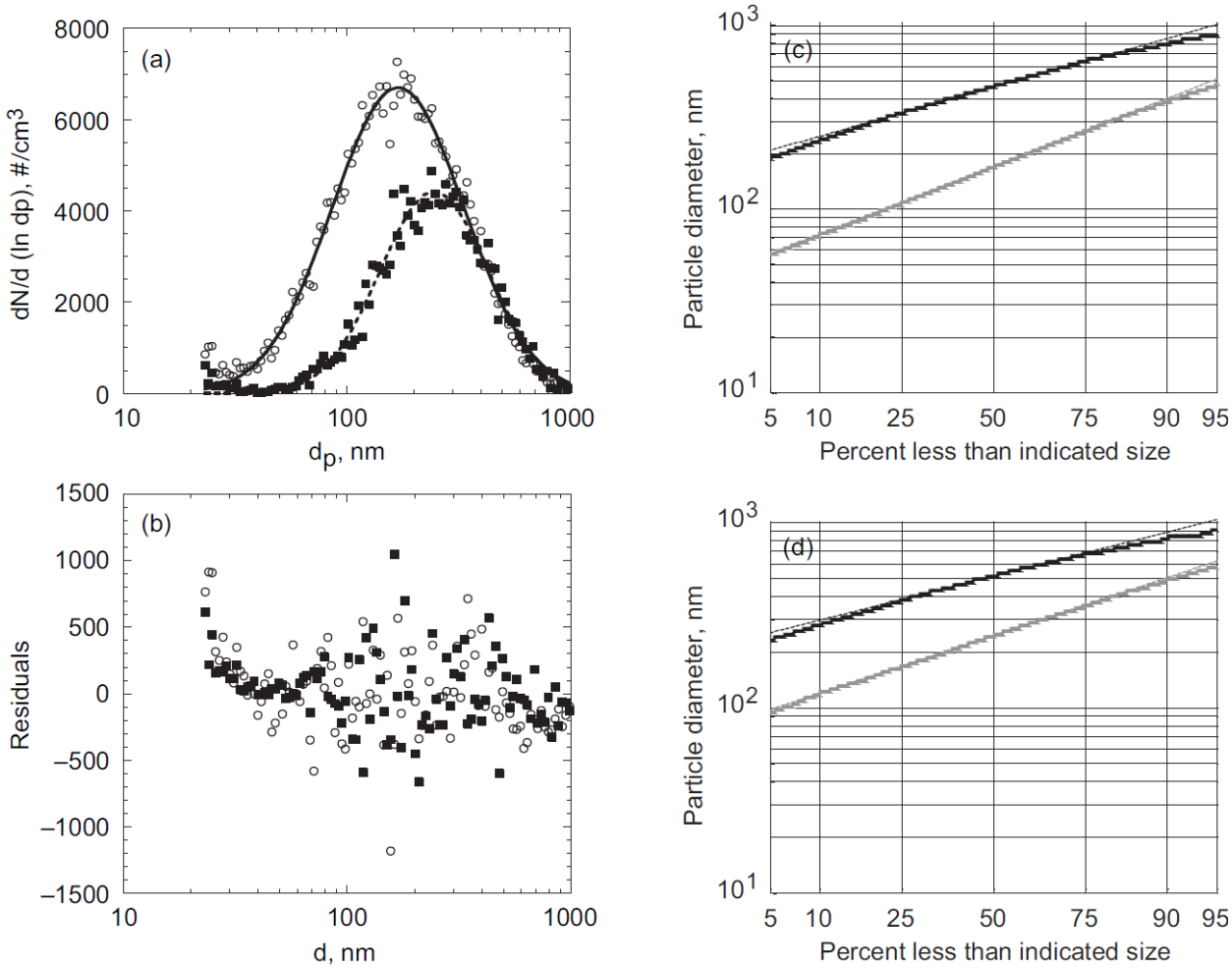

FIG. S7. (a) Smoke particle size distributions from SMPS measurements (ground tests) for a representative lamp wick high temperature test (286 °C) with open plot markers for unaged smoke (d_g = 171 nm, σ_g = 1.98) and solid symbols for aged smoke (d_g = 248 nm, σ_g = 1.75). The solid curves represent the non-linear least square fits. (b) A residual plot showing the deviations from the lognormal fits is aligned below the size distribution. Log-probability graphs for unaged (c) and aged (d), based on discrete SMPS bin data. Number distributions are grey, volume distributions are black, and dashed lines are lognormal curve fits.

Lamp wick log-probability plots are shown in Figures S7(c) and S7(d) (unaged and aged). The volume distributions have a smaller σ_g which is evident by the shallower slopes. This is caused by the limited SMPS measurement range, which misses a portion of the high

temperature lamp wick large diameter tail, a deficiency which is emphasized in the conversion to volume concentration. Log-probability plots for lamp wick demonstrate the flattening of the slope with aging, which corresponds to the narrowing of the distribution as coagulation takes place. The log-probability plots for silicone (Figures S8(c) and S8(d)) are not linear and thus fit a lognormal distribution poorly. The lognormal fit and the residual plot in Figures S8(a) and S8(b) reflect the same result, where the data are steeper than the fit curve for large diameters and less steep than the fit results for smaller diameters, thus the log-probability plot has deviations from the straight line fits at both the smallest and largest percentages of the distributions.

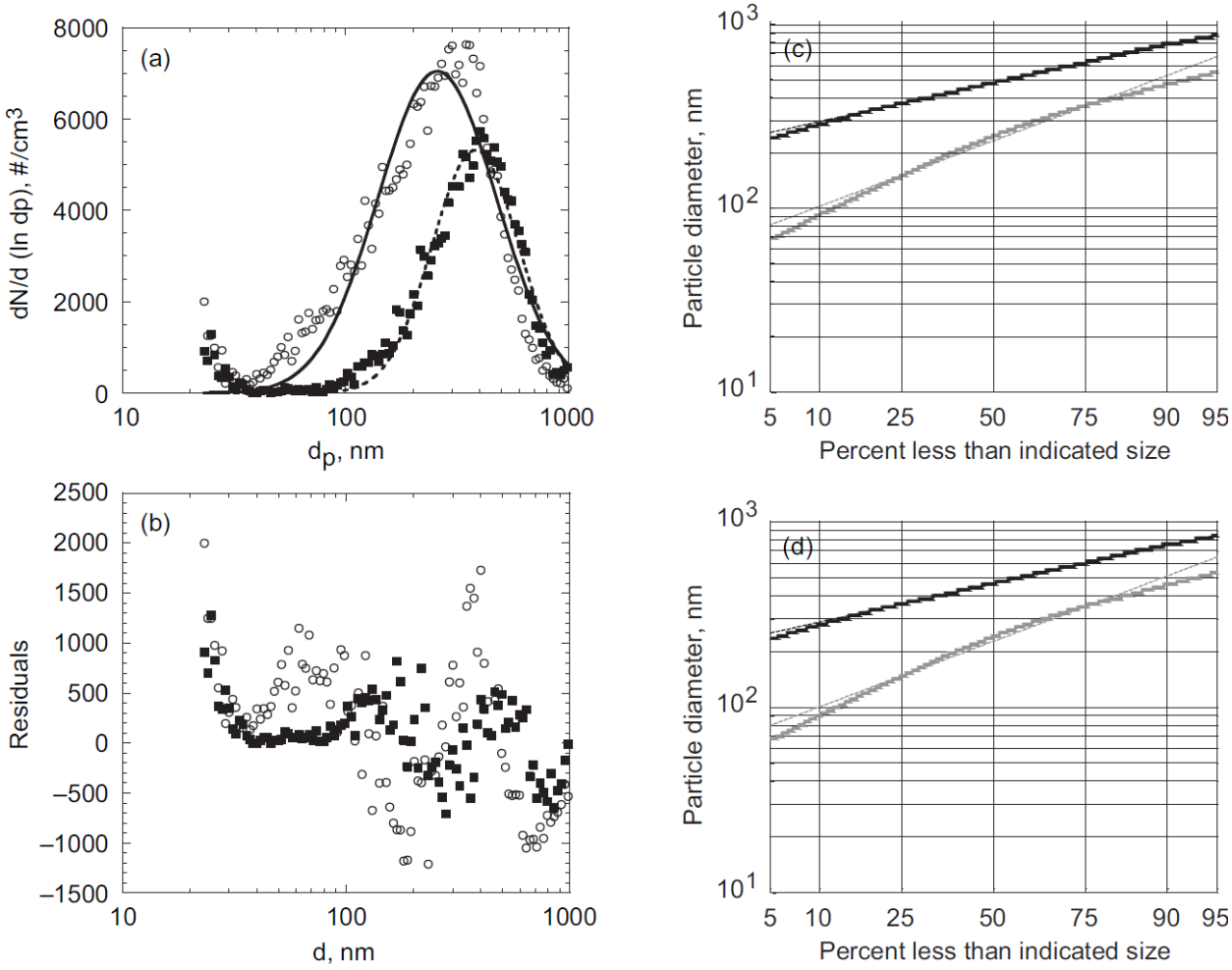

FIG. S8. (a) Smoke particle size distributions from SMPS measurements (ground tests) for a representative Silicone baseline temperature test (342 °C) with open plot markers for unaged smoke (d_g = 257 nm, σ_g = 1.84) and solid symbols for aged smoke (d_g = 382 nm, σ_g = 1.56). The solid curves represent the non-linear least square fits. (b) A residual plot showing the deviations from the lognormal fits is aligned below the size distribution. Log-probability graphs from unaged (c) and aged (d), based on discrete SMPS bin data. Number distributions are grey, volume distributions are black, and dashed lines are lognormal curve fits.

Pyrell TEM Particle Size Distribution

Pyrell size distributions are shown in Figure S7, which compares ISS TEM with SMPS ground testing. The TEM size distribution statistics of the unaged smoke are d_g = 249 nm and σ_g =1.84 (1970 particles counted) and after 14 minutes of aging, d_g increases to 328 nm and σ_g increases slightly to 1.98 (1627 particles counted). The SMPS size distribution statistics are d_g = 254 nm and σ_g =1.88 and after 14 minutes of aging, d_g increases to 364 nm and σ_g decreases slightly to 1.87. This comparison shows that the TEM projected area equivalent diameter is comparable to mobility diameter, even for non-spherical and agglomerate particles.

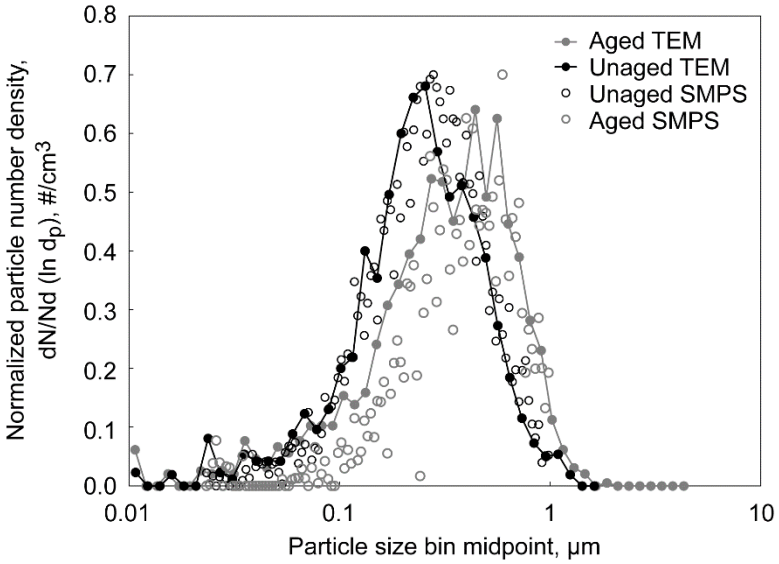

FIG. S9. Pyrell particle size distributions from TEM image analysis (projected area equivalent diameters) of ISS high temperature testing compared with SMPS size distributions from ground testing. Sample heating temperatures were 242 °C and 234 °C, respectively.

SMPS Results for Additional Temperature Conditions and Materials

Kapton is a low outgassing polyimide film that survives a wide temperature range and is used in electrical wire insulation and other spacecraft applications. The smoke particle size distribution of Kapton high temperature smoke is shown in Figure S10. SMPS results for lamp wick smoke at the baseline temperature are shown in Figure S11. SMPS results for silicone smoke at the high temperature condition are shown in Figure S12.

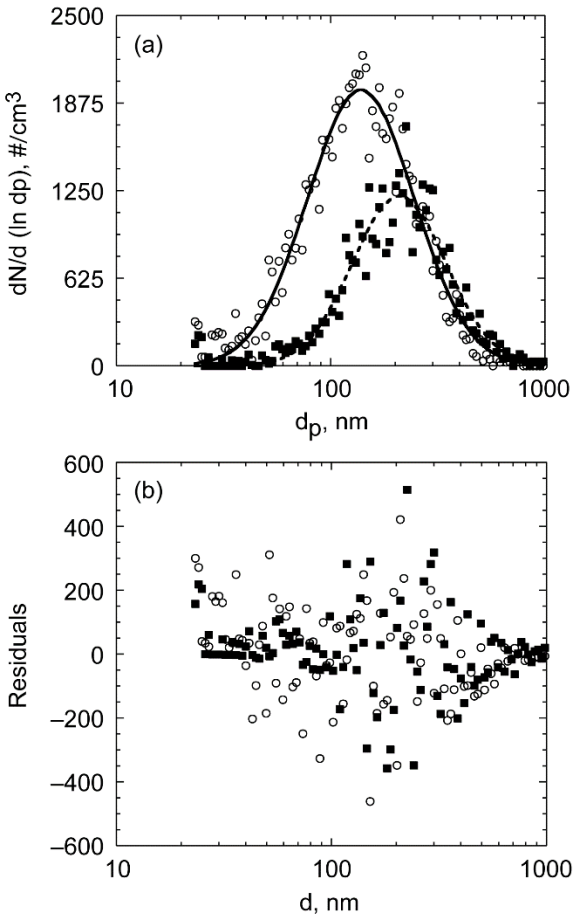

FIG. S10. (a) Smoke particle size distributions from SMPS measurements for a representative Kapton® high temperature test (557 °C) with open plot markers for unaged smoke (d_g = 140 nm, σ_g = 1.63) and solid symbols for aged smoke (d_g = 210 nm, σ_g = 1.55). The solid curves represent the non-linear least square fits. (b) Residual plot showing the deviations from the lognormal fits aligned below the size distribution.

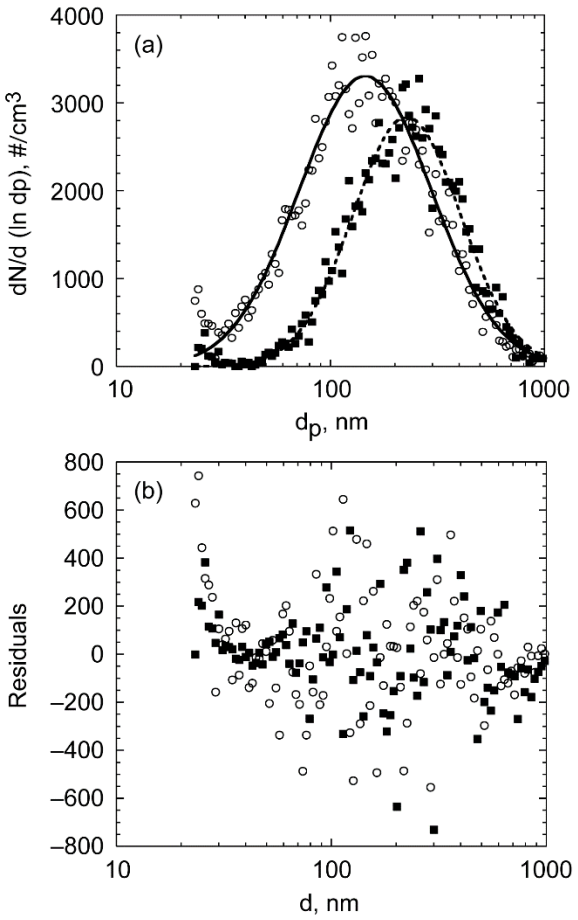

FIG. S11. (a) Smoke particle size distributions from SMPS measurements for a representative lamp wick baseline temperature test (250 °C) with open plot markers for unaged smoke (d_g = 146 nm, σ_g = 2.04) and solid symbols for aged smoke (d_g = 227 nm, σ_g = 1.79). The solid curves represent the non-linear least square fits. (b) Residual plot showing the deviations from the lognormal fits is aligned below the size distribution.

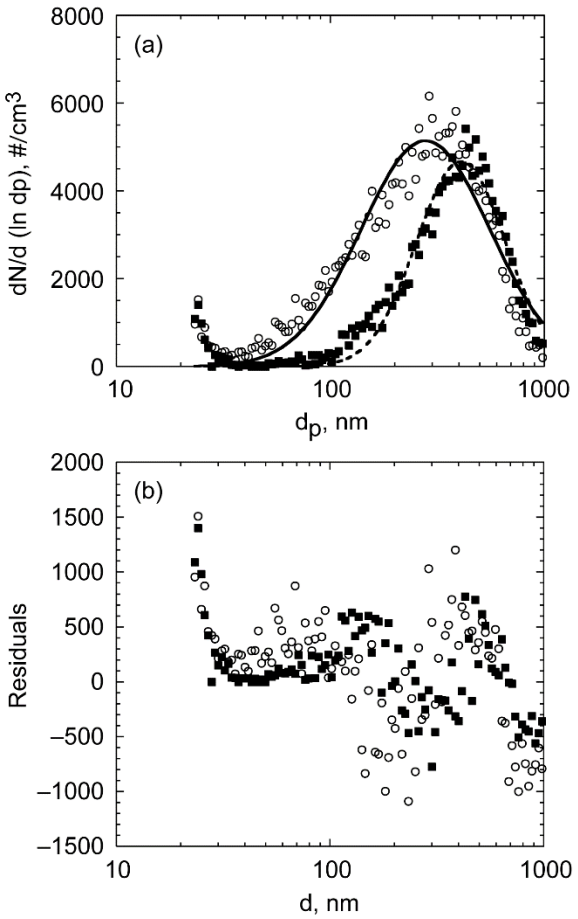

FIG. S12. (a) Smoke particle size distributions from SMPS measurements for a representative Silicone high temperature test (369 °C) with open plot markers for unaged smoke (d_g = 279 nm, σ_g = 2.00) and solid symbols for aged smoke (d_g = 409 nm, σ_g = 1.62). The solid curves represent the non-linear least square fits. (b) Residual plot showing the deviations from the lognormal fits aligned below the size distribution.

SMPS Results for Non-spherical Smoke Aerosols

Pyrell® is used for stowage foam to cushion instruments and other payloads during launch into space. Its widespread use made it a strong candidate in the survey of potential sources of smoke in spacecraft fires. Smoke particle size distributions for baseline and high temperature conditions are shown in Figure S13.

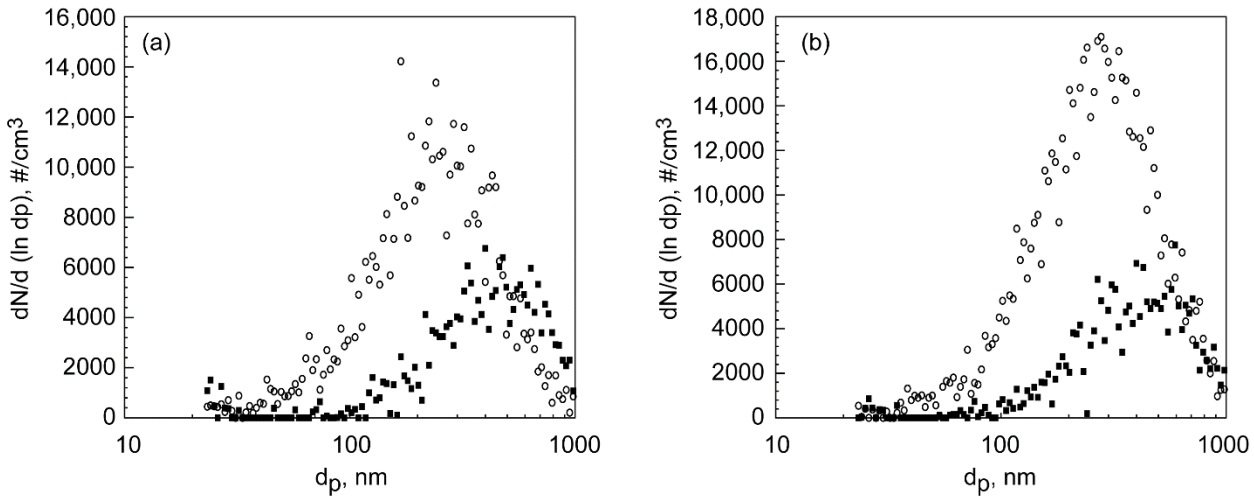

FIG. S13. Smoke particle size distributions from SMPS measurements for representative Pyrell® tests. (a) Baseline temperature (225 °C) with open plot markers for unaged smoke (d_g = 223 nm, σ_g = 1.93) and solid symbols for aged smoke (d_g = 370 nm, σ_g = 1.68). (b) High temperature (234 °C) with open plot markers for unaged smoke (d_g = 253 nm, σ_g = 1.88) and solid symbols for aged smoke (d_g = 364 nm, σ_g = 1.73).

Teflon® is present on the International Space Station in many forms, but predominantly in wire insulation. SMPS results for both baseline and high temperature tests are shown in Figure S14.

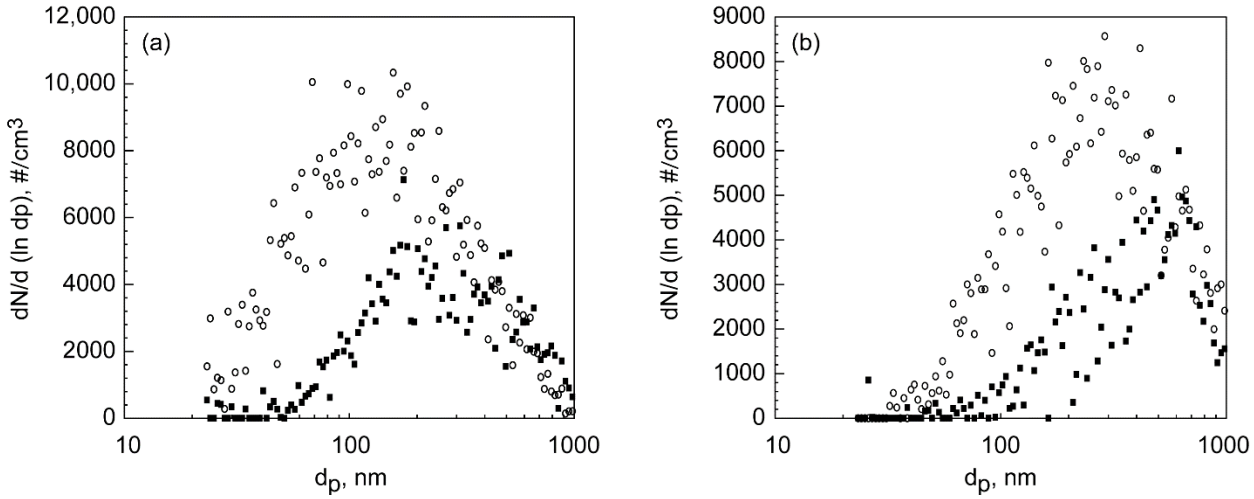

FIG. S14. Smoke particle size distributions from SMPS measurements for representative Teflon® tests. (a) Baseline temperature (501 °C) with open plot markers for unaged smoke (d_g = 139 nm, σ_g = 2.22) and solid symbols for aged smoke (d_g = 239 nm, σ_g = 2.02). (b) High temperature (512 °C) with open plot markers for unaged smoke (d_g = 248 nm, σ_g = 2.07) and solid symbols for aged smoke (d_g = 369 nm, σ_g = 1.90).

TEM Results from Flight tests

Results of the International Space Station (ISS) flight TEM size distribution analyses and moment method calculations appear in Table S1.

Table S1. Flight Data Comparison of TEM and Moment Method Distribution Parameters

Sample	Temperature, °C	# particles counted	D_m µm		D_{ave} µm		D_g µm		Sigma g		Hatch-Choate Diameters	
			TEM	Moment	TEM	Moment M1/M0	TEM D_{gn}	Moment	TEM σ_{gn}	Moment	Dav Hatch Choate from TEM sigma and Dg	Dm Hatch Choate from TEM sigma and Dg
Lampwick #54 (ISS) Unaged	Low Temp 264.7	511	0.403	0.253	0.304	0.11	0.255	0.072	1.84	2.493	0.307	0.445
Lampwick #55 (ISS) Aged	Low Temp 262.9	196	0.499	0.320	0.359	0.149	0.284	0.102	2.070	2.400	0.370	0.628
Kapton #94 (ISS) Aged	Low Temp 527.3	1353	0.159	0.176	0.120	0.136	0.103	0.119	1.720	1.669	0.119	0.160
Kapton #62 (ISS) Unaged	High Temp 574.3	1320	0.226	0.251	0.180	0.148	0.158	0.114	1.680	2.066	0.181	0.237
Kapton #62 (ISS) Aged	High Temp 574.3	796	0.289	0.383	0.235	0.243	0.210	0.194	1.630	1.962	0.237	0.300
Pyrell #63 (ISS) Unaged	Low Temp 225.3	3436	0.394	0.392	0.290	0.207	0.244	0.151	1.810	2.222	0.291	0.414
Pyrell #63 (ISS) Aged	Low Temp 225.3	2658	0.468	0.539	0.354	0.359	0.292	0.293	1.920	1.892	0.361	0.553
Pyrell #64 (ISS) Unaged	High Temp 242.1	1888	0.411	0.445	0.298	0.254	0.249	0.192	1.840	2.115	0.300	0.435
Pyrell #64 (ISS) Aged	High Temp 242.1	1560	0.540	0.616	0.403	0.450	0.328	0.385	1.980	1.750	0.414	0.660
Silicone #60 (ISS) Unaged	High Temp 379.9	557	0.153	0.533	0.120	0.241	0.107	0.162	1.590	2.440	0.119	0.148

REFERENCES

Chakrabarty, R. K., Moosmüller, H., Chen, L.-W. A., Lewis, K. A., Arnott, W. P., Mazzoleni, C., Dubey, M. K., Wold, C. E., Hao, W. M., Kreidenweis, S. M. (2010). Brown carbon in tar balls from smoldering biomass combustion. Atmos. Chem. Phys., 10, 6363–6370.

Chen, B. T., Namenyi, J., Yeh, H. C., Mauderly, J. L., Cuddihy, R. G. (1990). Physical Characterization of Cigarette Smoke Aerosol Generated from a Walton Smoke Machine. Aerosol Sci. Technol. 12:2, 364-375.

Cleary, T.G., Weinert, D.W., Mulholland, G.W., "Moment Method for Obtaining Particle Size Measures of Test Smokes," Natl. Inst. Stand. Technol., NISTIR 7050, 2003.

Fletcher, R.A. Mulholland, G.W., Winchester, M.R., King, R.L., and Klinedinst, D.B. (2009). Calibration of a Condensation Particle Counter Using a NIST Traceable Method, Aerosol Science and Technology, 43:425–441 (2009).

Hinds, W. C. (1999). Aerosol Technology, Second Edition, Wiley Interscience, New York.
Janhäll, S., Andreae, M. O., Pöschl, U. (2010). Biomass burning aerosol emissions from vegetation fires: particle number and mass emission factors and size distributions. Atmos. Chem. Phys., 10:1427–1439.
Li, W., Hopke, P. K. (1993). Initial Size Distributions and Hygroscopicity of Indoor Combustion Aerosol Particles. *Aerosol Sci. Technol.* 19:305-316.
Mack, L. A., Levin, E. J. T., Kreidenweis, S. M., Obrist, D., Moosmüller, H., Lewis, K. A., Arnott, W. P., McMeeking, G. R., Sullivan, A. P., Wold, C. E., Hao, W. M., Collett Jr., J. L. Malm, W. C. (2010). Optical Closure Experiments for Biomass Smoke Aerosols, Atmos. Chem. Phys., 10, 9017-9026.

Mulholland, G.W. and Liu, B.Y.H. (1980). "Response of Smoke Detectors to Monodisperse Aerosols," J. Research of the National Bureau of Standards, 85:223-238.
Raabe, O. G. (1971). Particle Size Analysis Utilizing Grouped Data and the Log-Normal Distribution, J. Aerosol Sci., 2:289-303.
Reist, P.C., Introduction to Aerosol Science, Macmillan Pub. Co., NY, NY, 1984.
Xie, Q., Yuan, H., Song, L., Zhang, Y. (2007). Experimental studies on time-dependent size distributions of smoke particles of standard test fires. Building and Environment 42:640-646.
Zai, S., Zhen, H., Jia-song, W. (2006). Studies on the size distribution, number and mass emission factors of candle particles characterized by modes of burning. Jour. Aerosol Sci. 37:1484-1496.